Monthly Notices of the ROYAL ASTRONOMICAL SOCIETY

MNRAS **515,** 3773–3795 (2022)
Advance Access publication 2022 July 22

https://doi.org/10.1093/mnras/stac1983

# Von Zeipel – Lidov – Kozai cycles in action: *Kepler* triples with eclipse depth variations: KICs 6964043, 5653126, 5731312, and 8023317

T. Borkovits [1,2,3,4,5★] S. A. Rappaport,[6] S. Toonen,[7] M. Moe,[8] T. Mitnyan[1,2] and I. Csányi[1]

[1]*Baja Astronomical Observatory of University of Szeged, H-6500 Baja, Szegedi út, Kt. 766, Hungary*
[2]*ELKH-SZTE Stellar Astrophysics Research Group, H-6500 Baja, Szegedi út, Kt. 766, Hungary*
[3]*Konkoly Observatory, Research Centre for Astronomy and Earth Sciences, H-1121 Budapest, Konkoly Thege Miklós út 15-17, Hungary*
[4]*ELTE Gothard Astrophysical Observatory, H-9700 Szombathely, Szent Imre h. u. 112, Hungary*
[5]*MTA-ELTE Exoplanet Research Group, H-9700 Szombathely, Szent Imre h. u. 112, Hungary*
[6]*Department of Physics, Kavli Institute for Astrophysics and Space Research, M.I.T., Cambridge, MA 02139, USA*
[7]*Anton Pannekoek Institute for Astronomy, University of Amsterdam, NL-1090 GE Amsterdam, the Netherlands*
[8]*University of Arizona, Steward Observatory, 933 N. Cherry Ave., Tucson, AZ 85721, USA*

Accepted 2022 July 11. Received 2022 July 9; in original form 2022 May 25

## ABSTRACT

We report the results of the photodynamical analyses of four compact, tight triple stellar systems, KICs 6964043, 5653126, 5731312, and 8023317, based largely on *Kepler* and *TESS* data. All systems display remarkable eclipse timing and eclipse depth variations, the latter implying a non-aligned outer orbit. Moreover, KIC 6964043 is also a triply eclipsing system. We combined photometry, ETV curves, and archival spectral energy distribution data to obtain the astrophysical parameters of the constituent stars and the orbital elements with substantial precision. KICs 6964043 and 5653126 were found to be nearly flat with mutual inclinations $i_{\rm mut} = 4\overset{\circ}{.}1$ and $12\overset{\circ}{.}3$, respectively, while KICs 5731312 and 8023317 ($i_{\rm mut} = 39\overset{\circ}{.}4$ and $55\overset{\circ}{.}7$, respectively) are found to lie in the high $i_{\rm mut}$ regime of the von Zeipel-Kozai-Lidov (ZKL) theorem. We show that, currently, both high inclination triples exhibit observable unusual retrograde apsidal motion. Moreover, the eclipses will disappear in all but one of the four systems within a few decades. Short-term numerical integrations of the dynamical evolution reveal that both high inclination triples are currently subject to ongoing, large amplitude ($\Delta e \sim 0.3$) inner eccentricity variations on centuries-long time-scales, in accord with the ZKL theorem. Longer-term integrations predict that two of the four systems may become dynamically unstable on $\sim$ Gyr time-scales, while in the other two triples common envelope phases and stellar mergers may occur. Finally, we investigate the dynamical properties of a sample of 71 KIC/TIC triples statistically, and find that the mutual inclinations and outer mass ratios are anticorrelated at the $4\sigma$ level. We discuss the implications for the formation mechanisms of compact triples.

**Key words:** binaries: close – binaries: eclipsing – stars: individual: KIC 6964043 – stars: individual: KIC 5653126 – stars: individual: KIC 5731312 – stars: individual: KIC 8023317.

## 1 INTRODUCTION

The advent of planet-hunter space telescopes, such as *CoRoT* (Auvergne et al. 2009), *Kepler* (Borucki et al. 2010), and *TESS* (Ricker et al. 2015), has additionally opened up a new window for the detection of exotic multiple stellar systems. This especially includes triple systems and quadruples, which are both 'compact' and 'tight'. For simplicity, considering only hierarchical triple systems, by 'compactness' we mean that the outer orbital period does not exceed, let's say $P_{\rm out} = 1000$ d, while a triple system is said to be 'tight' for an outer to inner period ratio $P_{\rm out}/P_{\rm in} \leq 100$.[1] Tightness is important because the magnitude of the gravitational three-body perturbations in a hierarchical triple stellar system, relative to the Keplerian motion, is primarily determined by the ratio of semimajor axes of the inner and outer orbits. This ratio, with the use of Kepler's third law, can easily be converted to the ratio of the much easier-to-observe orbital periods. On the other hand, compactness, which is closely connected to the physical dimensions of the system, strongly influences the time-scale of three- (multiple-) body perturbations. Moreover, tightness is also important in determining the relations of the magnitudes of other kinds of perturbations, e.g. tidal and relativistic, to the dynamical ones, since these other perturbations primarily scale with the semimajor axis, i.e. the compactness of the system. Finally, in this regard, compactness is also an important parameter because, according to our present knowledge, compact multiple systems form and evolve in a different manner than their wider counterparts (see e.g. Tokovinin 2021, in the sense of their formation, and Toonen et al. 2020, 2022, in regard of their later evolution).

Hierarchical triple systems exhibit periodic gravitational perturbations in three different, well separable time-scales. (i) The shortest period ones act on the time-scale of the inner orbit ($P_{\rm in}$), and have a relative amplitude on the order of the ratio $(P_{\rm in}/P_{\rm out})^2$ and thus, this class of perturbations is hardly observable. (ii) The medium time-scale class of periodic perturbations have characteristic periods

★ E-mail: borko@electra.bajaobs.hu

[1]Note, however, that these numerical values were chosen somewhat arbitrarily, and we do not mean to attempt to impose strict limits.

on the order of the period of the outer orbit ($P_{\rm out}$) and relative magnitude of $P_{\rm in}/P_{\rm out}$ (i.e. longer in period and larger in amplitude than the short-period ones by a factor of $P_{\rm out}/P_{\rm in}$). (iii) Finally, the long-period (or, according to another nomenclature, the 'apse-node' type) perturbations have a time-scale related to $P_{\rm out}^2/P_{\rm in}$ and relative amplitude of unity[2] (i.e. yet longer/larger than the previous perturbations, with a second factor of $P_{\rm out}/P_{\rm in}$.)

In terms of the formation, evolution, and future fate and stability of hierarchical stellar systems, the largest amplitude, long-period perturbations are by far the most important. Therefore, it is not surprising that theoretical studies of the stellar third-body problem have focused almost exclusively on long-period perturbations (see e.g, the recent review of Naoz 2016, and further references therein).

Perhaps the most spectacular consequence of these long-period perturbations occurs in the case of highly inclined inner and outer orbital planes. The eccentricity of the inner orbit may then alternate periodically between small values (including zero) and nearly unity and, in parallel with this, the mutual inclination of the orbits also varies substantially in an anticorrelated manner. In recent years, these effects are frequently referred as 'von Zeipel-Lidov-Kozai effects' (hereafter ZLK) or 'ZLK oscillations or, cycles' in the honour of its first investigators (von Zeipel 1910; Kozai 1962; Lidov 1962)[3]

The original ZLK theorem takes into account only the lowest order quadrupole, long-period perturbations, and is strictly valid only if the orbital angular momentum of the triple system is stored exclusively in the outer orbit, which is also circular. This asymptotic quadrupole ZKL theorem has only one degree of freedom and, hence, is integrable; therefore, the variations of the inner eccentricity ($e_{\rm in}$), dynamical argument of periastron ($\omega_{\rm in}^{\rm dyn}$), and mutual inclination ($i_{\rm mut}$) can be given in closed form. Based on the analytic form of the perturbation equations, it can readily be shown that the behaviour of the ZKL cycles may be essentially divided into two mutual inclination regimes, which are separated by the value of $|\cos i_{\rm mut}| = \sqrt{3/5}$, i.e. $i_{\rm mut} \approx 39\overset{\circ}{.}23$ and its retrograde counterpart.[4] Below this mutual inclination (i.e. in the low mutual inclination regime), there may occur only small-amplitude variations in the inner eccentricity and the mutual inclination as well. Furthermore, in the case of an initially circular inner orbit, it remains circular at all times (of course, only in so far as the approximation used remains valid).

In the high mutual inclination case, depending on the initial conditions, (i.e. the value of the inner binary eccentricity, mutual inclination, and dynamical argument of pericenter at a given instant), the inner eccentricity and the mutual inclination may oscillate with large amplitudes, while the apsidal line may exhibit either circulation or libration. As an extreme example, an originally circular inner orbit, perturbed by a tertiary orbiting perpendicular to its orbit (i.e. $i_{\rm mut} = 90^\circ$), may have its eccentricity periodically grow to near unity and then shrink back to zero while, at the same time, the mutual inclination oscillates between $\cos^2 i_{\rm mut} = 0$ and $\cos^2 i_{\rm mut} = 3/5$. Taking into consideration the further octupole terms of the perturbation function, and allowing the third body to have any arbitrary eccentricity, e.g. Ford, Kozinsky & Rasio (2000) and Naoz et al. (2013) have shown that the problem will no longer be analytically integrable, and the behaviour of the orbital elements may be more complex. For example, large eccentricity variations may already occur in the case of lower mutual inclination triples, the relative orientations of the orbital planes may show flip-flop phenomena between prograde and retrograde orientations, the semimajor axis of the inner orbit may alternate between libration and circulation, and so forth.

Although the large-amplitude ZLK eccentricity cycles are evidently the most important long-period, or secular, effects in the formation and evolution of triple star systems, these are often barely observable in action. The main reason is that, due to their typically long time-scale, one cannot expect measurable eccentricity variations from spectroscopic, photometric, or astrometric observations[5] on time-scales of years or decades. Fortunately, however, in the case of some other orbital elements, the variations driven by the very same mechanism (i.e. third-body perturbations) may lead to readily observable effects even on 'astronomer career' time-scales. These long-period perturbations are (i) the third-body forced apsidal motion (in the case of an eccentric inner binary) and (ii) the orbital plane precession (or, nodal regression) in those triple systems where the inner and outer orbital planes are not aligned. (Hence the other name of 'apse-node time-scale perturbations').

Eclipsing binaries (EBs) that belong to tight and compact hierarchical triple and multiple stellar systems may be ideal for the detection of both of these effects. In particular, they can provide important information on the non-alignment of the orbital planes, or, oppositely, the flatness of the given systems. This is the case because the orbital plane precession, in the case of an EB, leads to a variation in the eclipse depths and, even to the disappearance of former eclipses or, in the opposite sense, the occurrence of eclipses in formerly non-EBs. The characteristic time-scale of this effect for triples can be estimated by the following simple expression (Söderhjelm 1975):

$$P_{\rm node} = \frac{4}{3}\frac{1+q_{\rm out}}{q_{\rm out}}\frac{P_{\rm out}^2}{P_{\rm in}}\left(1-e_{\rm out}^2\right)^{3/2}\left|\frac{C}{G_{\rm out}}\cos i_{\rm mut}\right|^{-1}, \qquad (1)$$

where $q_{\rm out}$ represents the outer mass ratio, $P_{\rm in,\,out}$ denote the periods of the inner and outer orbits, $e_{\rm out}$ stands for the outer eccentricity, and $C$ is the (constant) total orbital angular momentum of the triple, while $G_{\rm out}$ stands for the orbital angular momentum stored in the outer orbit and, finally, $i_{\rm mut}$ the mutual (relative) inclination of the two orbital planes.

From an observational point of view, however, the problem is that, although the stability of a hierarchical triple stellar system allows for very tight configurations with $P_{\rm out}/P_{\rm in} \approx 5$ (see e.g. Mardling & Aarseth 2001), in the vast majority of known triple or multiple systems that contain an EB, this ratio is larger than 100. Moreover, because the periods of the outer stellar components are typically longer than 1 yr, the time-scale of the precession, and therefore the variation of the eclipse depths, may reach several centuries or, millennia, in most of the systems. Therefore, one might expect eclipse depth variations (EDVs) that occur rapidly enough to be observable during the ≈1.5 century-long history of EB observations, only in the

[2]Unity is to be meant in that sense, that during the time-scale of the long-period perturbations, the numerical value of a given orbital element may take any numerical value within its physical range.

[3]These early authors did not deal with the hierarchical three-body problem in the context of stellar triple systems, but, instead studied the motions of small bodies in triple systems (e.g. perturbations of Jupiter from comets and asteroids orbiting around the Sun – von Zeipel; Kozai; or perturbations of the Moon for Earth-orbiting artificial satellites – Lidov; see the recent monograph of Ito & Ohtsuka 2019). The first analytic works on this theorem, dedicated directly to the stellar three-body problem was published by Harrington (1968) and Söderhjelm (1982).

[4]Within the framework of the original ZKL theorem, the prograde and retrograde configurations are equivalent.

[5]At least within the accuracy limits of instruments that are commonly available for observing hierarchical triple stellar systems.

**Table 1.** Main properties of the three systems from different catalogs.

| Parameter | 6964043 | 5653126 | 5731312 | 8023317 |
|---|---|---|---|---|
| RA (J2000) | 19: 44: 03.474 | 19: 58: 48.479 | 19: 53: 00.434 | 19: 19: 52.879 |
| Dec (J2000) | +42: 25: 20.09 | +40: 53: 46.51 | +40: 54: 12.77 | +43: 49: 13.84 |
| $G^b$ | 15.5868 ± 0.0003 | 13.1434 ± 0.0001 | 13.8246 ± 0.0001 | 12.8453 ± 0.0002 |
| $G^b_{\rm BP}$ | 16.0472 ± 0.0029 | 13.5364 ± 0.0007 | 14.3641 ± 0.0008 | 13.2064 ± 0.0005 |
| $G^b_{\rm RP}$ | 14.9591 ± 0.0014 | 12.5802 ± 0.0004 | 13.1272 ± 0.0005 | 12.3194 ± 0.0005 |
| $B^a$ | 16.307 ± 0.068 | 14.159 ± 0.026 | 15.030 ± 0.066 | 13.819 ± 0.036 |
| $V^a$ | 16.007 ± 0.137 | 13.225 ± 0.069 | 14.035 ± 0.103 | 12.990 ± 0.069 |
| $g'$ | 16.007 ± 0.071$^c$ | 13.709 ± 0.014$^d$ | 14.584 ± 0.001$^e$ | 13.329 ± 0.031$^d$ |
| $r'$ | 15.533 ± 0.048$^c$ | 13.139 ± 0.035$^d$ | 13.659 ± 0.001$^e$ | 12.810 ± 0.045$^d$ |
| $i'$ | 15.276 ± 0.083$^c$ | 13.028 ± 0.093$^d$ | 13.069 ± 0.001$^e$ | 12.702 ± 0.028$^d$ |
| $J^f$ | 14.231 ± 0.027 | 11.957 ± 0.021 | 12.242 ± 0.022 | 11.682 ± 0.023 |
| $H^f$ | 13.758 ± 0.026 | 11.710 ± 0.022 | 11.729 ± 0.023 | 11.395 ± 0.020 |
| $K^f$ | 13.705 ± 0.043 | 11.632 ± 0.020 | 11.598 ± 0.018 | 11.340 ± 0.011 |
| $W1^g$ | 13.658 ± 0.025 | 11.543 ± 0.023 | 11.559 ± 0.024 | 11.310 ± 0.023 |
| $W2^g$ | 13.680 ± 0.031 | 11.572 ± 0.021 | 11.611 ± 0.023 | 11.359 ± 0.021 |
| $W3^g$ | 13.061 | 11.595 ± 0.122 | 12.926 | 11.163 ± 0.094 |
| $W4^g$ | 9.614 | 8.897 | 9.458 | 9.442 |
| $T_{\rm eff}$ (K)$^a$ | 5445 ± 122 | 6980 ± 118 | 4885 ± 60 | 5638 ± 103 |
| Distance (pc)$^h$ | 2162 ± 142 | 1296 ± 32 | 351 ± 3 | 753 ± 7 |
| $[M/H]^a$ | – | 0.435 ± 0.111 | −0.372 ± 0.057 | 0.224 ± 0.016 |
| $E(B-V)^a$ | 0.130 ± 0.008 | 0.213 ± 0.014 | 0.073 ± 0.024 | 0.035 ± 0.002 |
| $\mu_\alpha$ (mas yr$^{-1}$)$^b$ | −2.95 ± 0.03 | 0.38 ± 0.02 | 1.69 ± 0.03 | −4.25 ± 0.01 |
| $\mu_\delta$ (mas yr$^{-1}$)$^b$ | −1.69 ± 0.04 | −1.12 ± 0.02 | 5.58 ± 0.03 | −1.09 ± 0.01 |

$^a$TESS Input Catalog (TIC v8.2) (Paegert et al. 2021). $^b$Gaia EDR3 (Gaia collaboration 2021). $^c$AAVSO Photometric All Sky Survey (APASS) DR10, (Henden 2019), https://www.aavso.org/download-apass-data. $^d$AAVSO Photometric All Sky Survey (APASS) DR9, (Henden et al. 2015), http://vizier.u-strasbg.fr/viz-bin/VizieR?-source = II/336/apass9. $^e$The Kepler-INT survey (Greiss et al. 2012). $^f$2MASS catalog (Skrutskie et al. 2006). $^g$WISE point source catalog (Cutri et al. 2013). $^h$Bailer-Jones et al. (2021).
Note also, that for the SED analysis in Section 4, the uncertainties of the pass-band magnitudes were set to $\sigma_{\rm mag} = \max(\sigma_{\rm catalog}, 0.030)$ to avoid the strong overdominance of the extremely accurate Gaia magnitudes over the other measurements.

most compact, tightest, and relatively rare (Tokovinin 2014) triple systems.

Consequently, it is hardly surprising that before the era of the long-duration, ground-based and space-borne photometric surveys, EDVs were (serendipitously) detected in only fewer than a dozen EBs (see the recent review of Borkovits 2022). In contrast to this, Kirk et al. (2016) listed 43 EBs in the original *Kepler* sample that exhibit EDVs. Though some of their systems were probably false positives (for a number of different reasons), on the other hand, they did not list some EBs with evident EDVs (e.g. neither KIC 6964043, nor KIC 5731312, two of our four systems that are analysed in this paper). Therefore, we may confidently state that the number of the EBs with known EDVs had more than tripled by the end of the 4-yr-long primary mission of the *Kepler* space telescope. The majority of these EDV-exhibiting EBs in the *Kepler*-field also display rapid apsidal motion. Moreover, they have readily detectable medium-period eclipse timing variations (ETV) which are, again, forced by the dynamical effects (DE) of the third body (besides, and instead of, the usual, well-known light-travel-time effect – LTTE, Rappaport et al. 2013; Borkovits et al. 2015, 2016). Therefore, these systems offer excellent opportunities to determine their complete geometric and dynamical configurations with unexpectedly high precision through complex, photodynamical analyses. In this manner, these triple stellar systems may serve as actual case studies for later, in-depth investigations of the formation, as well as past, present, and future evolutions of hierarchical triple star systems.

In Section 2, we introduce the four triples selected for our present investigations, and we discuss the prior results on these systems that are relevant in the context of the present study. Then the description of the observational data and their preparation can be found in Section 3, while the applied photodynamical method is summarized in Section 4. In Section 5, we discuss the results of the photodynamical analyses, and study the future dynamical and astrophysical evolutions of each system based on these results. Moreover, the implications of our present and former findings about compact triple star systems for the formation processes of multiple star systems are also discussed on a statistical basis. Finally, general concluding remarks are made in Section 6.

## 2 SELECTED SYSTEMS

In a previous work, Borkovits et al. (2015) analysed 26 such eccentric EBs in the original *Kepler*-field for which perturbations by a close tertiary star dominated the ETV. Amongst these triples, 17 were found to exhibit EDVs to differing degrees, indicating that the tertiary star has an inclined orbit relative to the plane of the inner binary. We have selected four targets of these 17 systems for a detailed analysis. According to the previous analytic ETV analysis of Borkovits et al. (2015), two of the four systems belong to the low mutual inclination regime and, hence, one can expect rapid, but small-amplitude medium and long-period variations in the orbital elements. By contrast, the other two systems belong to the rare class of highly inclined close triples, with $i_{\rm mut}$ close to the inclination limit of the asymptotic, quadrupole ZKL theory. Therefore, they may be ideal for direct observational detections of such exotic perturbation effects, as, e.g. rapid, strong eccentricity variations and/or retrograde (or, librating) apsidal motion. The main cataloged parameters of the systems are tabulated in Table 1, while their 4-yr-long *Kepler* light

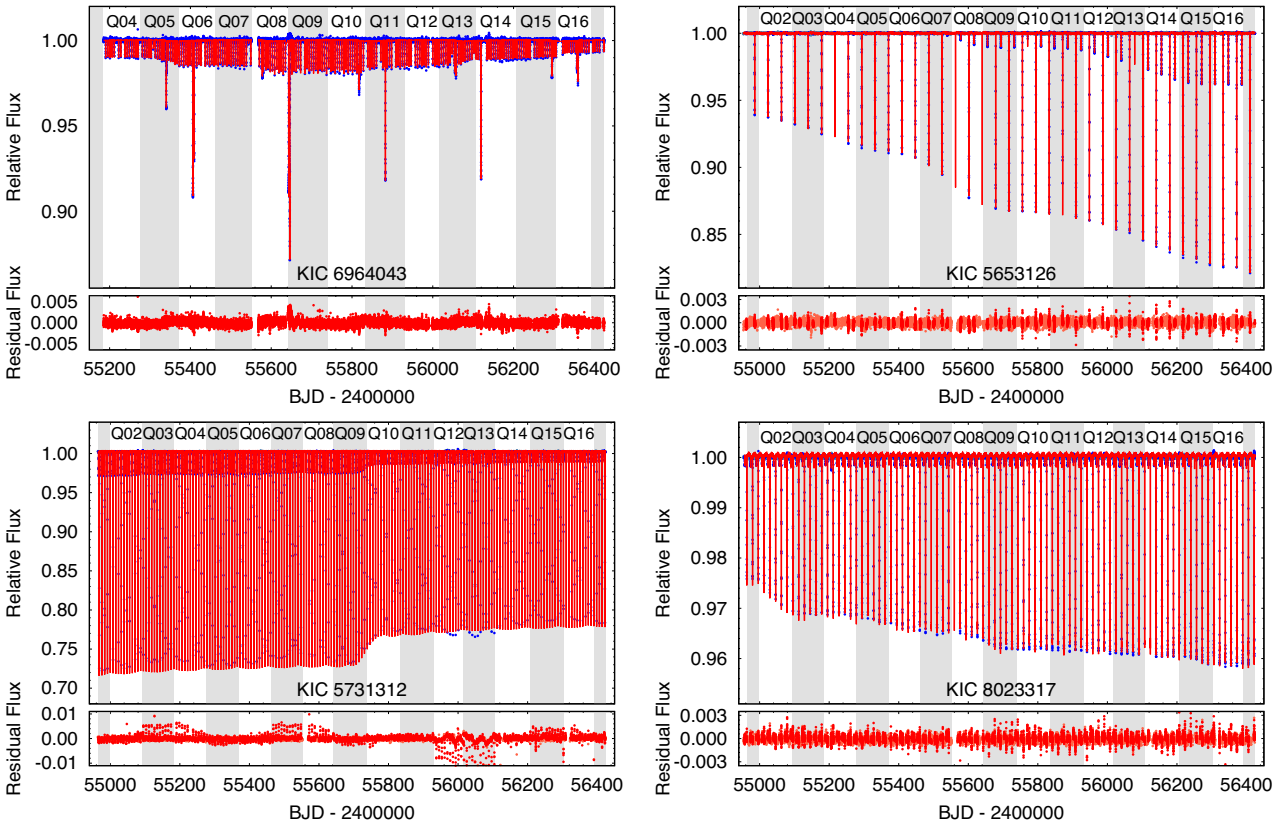


**Figure 1.** 4-yr long *Kepler* long cadence light curves of the four investigated systems with the photodynamical model solution. Small blue circles are the data points while the continuous red curves are the photodynamical models. Note, the alternating grey-white stripes help to distinguish the observing quarters.

curves are plotted in Fig. 1. Below we summarize the main properties found from their prior results for these four systems individually. Because we are mainly interested in the consequences of the inclined inner and outer orbital planes, we list the systems throughout this paper in the order of increasing value of the mutual inclination ($i_{\rm mut}$) parameter as it is obtained from the present study.

*KIC 6964043 = KOI-1351* ($P_1 = 10.73$ d; $P_2 = 239$ d; $P_2/P_1 = 22.3$) was observed by *Kepler* in long cadence (LC) mode only from the fourth quarter (Q4) of the primary mission to its end (Q17). Moreover, it was also observed in 1-min short cadence (SC) mode in Q12. It is the only triply eclipsing triple system in our sample. These extra, third-body eclipses are the largest amplitude, longest duration features of the light curve (see upper-left panel of Figs 1–3). The regular inner eclipses are quite shallow (with depths of $\sim$1−2 per cent). The inner EB exhibits growing eclipse depths during the first few quarters and then, after a short period of constancy, the eclipse depths continuously decrease. This is the most compact and tightest triple in our sample. Borkovits et al. (2015) have investigated the ETV of the EB and pointed out that it is clearly dominated by DE, i.e. third-body perturbations over the LTTE. Therefore, besides the orbital elements and mass ratio of the outer orbit, they were able to determine the full spatial configuration of the triple and, hence, the mutual inclination and got $i_{\rm mut} = 19^\circ \pm 2^\circ$[6] Moreover, they estimated the periods of both the apsidal motion and the nodal regression to be about 26–27 yr. KIC 6964043 was also observed with *TESS* in full-frame image (FFI) mode in sectors 14 and 15, but these observations exhibit neither regular inner eclipses, nor third-body eclipses, which is in accord with our photodynamical model, as will be discussed below in Section 5.

*KIC 5653126 = KOI-6612* ($P_1 = 38.51$ d; $P_2 = 968$ d; $P_2/P_1 = 25.1$) has by far the longest inner period of all the triples in our sample. It was observed throughout the original *Kepler*-mission ($Q0 - Q17$) in LC mode, while SC data are also available for quarters $Q9 - Q17$. The EB exhibits continuously increasing eclipse depths. In the first seven quarters, only primary eclipses were observable. The first, very shallow, grazing secondary eclipse with a depth of $\sim$0.002 per cent can be identified at BJD 2 455 539.7 (near the end of $Q7$). During the second half of the data train, both kinds of eclipses can be clearly detected (see upper-right panel of Fig. 1 and left-hand panel of Fig. 4). Borkovits et al. (2015) found a mutual inclination of $i_{\rm mut} = 11^\circ \pm 1^\circ$ and apsidal motion and nodal periods on the order of 2–3 centuries. The system was also observed by the *TESS* spacecraft in FFI-mode during Sectors 14, 15, and 41, where the observations led to the detection of one additional primary, and three secondary eclipses. The 2019 summer (S14,15) observations show flat-bottomed eclipses, while the somewhat shallower 2021 (S41) secondary eclipse is again V-shaped, indicating that the eclipse depths are now decreasing after an interval of total eclipses (right-hand panel of Fig. 4).

*KIC 5731312 = KOI-6621* ($P_1 = 7.95$ d; $P_2 = 911$ d; $P_2/P_1 = 114.6$) is the shortest inner period triple in our sample. Similar to KIC 5653126, it was observed throughout the original *Kepler*-mission ($Q0 - Q17$) in LC mode. One quarter ($Q10$) of SC data

[6]Note, that in contrast to the other three systems, where our new results confirm the mutual inclinations obtained from the prior pure ETV analysis of Borkovits et al. (2015), in the case of this triple the present, more complex study (see later in Section 4) resulted in a much lower value of $i_{\rm mut} = 4\overset{\circ}{.}1 \pm 0\overset{\circ}{.}1$.

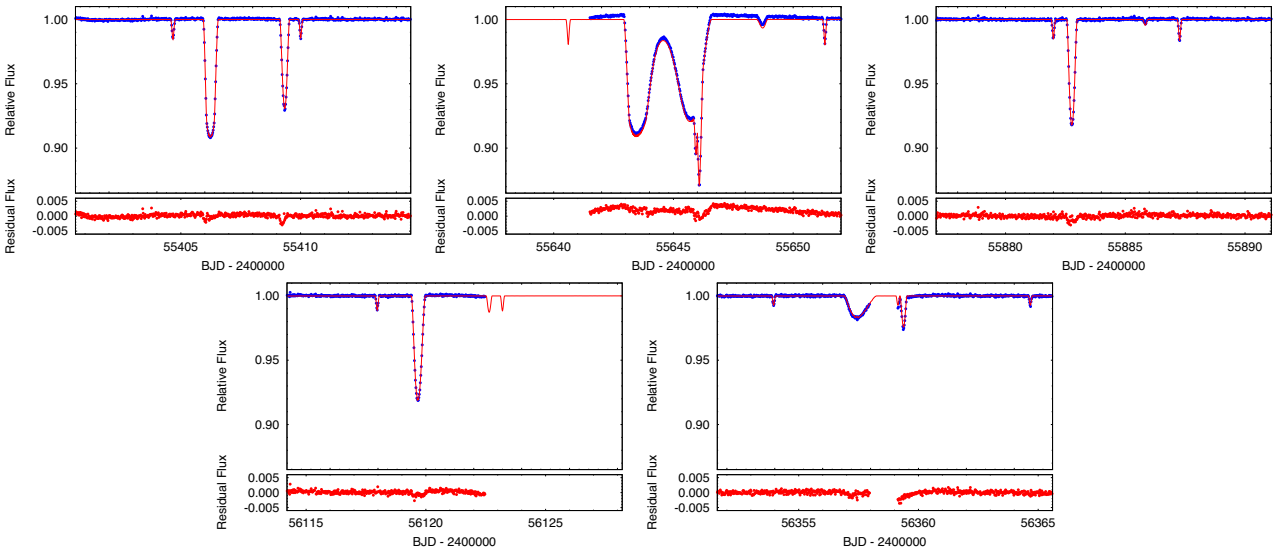


**Figure 2.** The 'primary' third-body, or outer eclipses of KIC 6964043 observed with *Kepler*. During these events the two red dwarfs of the inner binary transit (either partially or, totally) in front of the disc of the outer, most massive, G-star component. Blue dots represent the observed LC fluxes, while red lines represent the best-fitting photodynamical model.

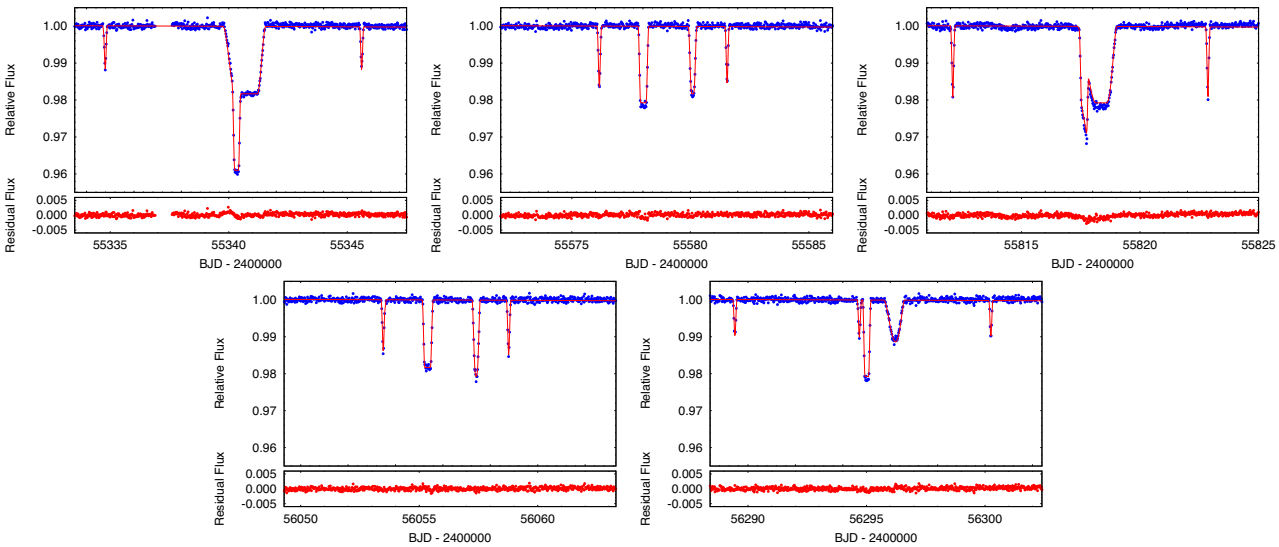


**Figure 3.** The 'secondary' third-body, or outer eclipses of KIC 6964043 observed with *Kepler*. During these events the two red dwarfs of the inner binary are eclipsed (either partially or, totally) by the outer, most massive, G-star component. Blue dots represent the observed LC fluxes, while red lines represent the best-fitting photodynamical model.

are available as well. During the *Kepler* observations, this system exhibited the deepest primary eclipses amongst the four systems. During the first half of the observations, only a small smooth decrease in the amplitude of the eclipses can be observed (which is nearly obscured by a wave-like pattern which, however, is only a beating effect between the data sampling and the eclipsing periods). Then, between BJDs 2455700 and 800, a sudden decrease in eclipse depths occurred, which was then again followed by a slow smooth decrease. The much shallower secondary eclipses followed the same trend (see lower left-hand panel of Fig. 1 and left-hand panel of Fig. 5). At the same time, the primary and secondary ETV curves also exhibited dramatic peaked variations, clearly indicating periastron passage of the eccentric third body. Note, despite the fact that the outer to inner period ratio exceeds 100, the ETV curves of this EB are clearly dominated by the DE over the LTTE. Borkovits et al. (2015) and, in their slightly revised ETV-analysis Borkovits et al. (2016), also found that this triple system is probably quite inclined with a mutual inclination of $i_{\rm mut} = 37\overset{\circ}{.}8 \pm 0\overset{\circ}{.}4$. In addition, their analytical model fit resulted in a currently retrograde apsidal motion. The EB was also observed with *TESS* in sectors 14, 15, and 41. By this time, the secondary eclipses had disappeared, which is again in accord with our photodynamical results to be presented below. Moreover, in between the 2019 and 2021 space telescope observations, two additional primary eclipses were also observed at Baja Observatory, Hungary, within the framework of our photometric *Kepler* and *TESS* EB follow-up programme.

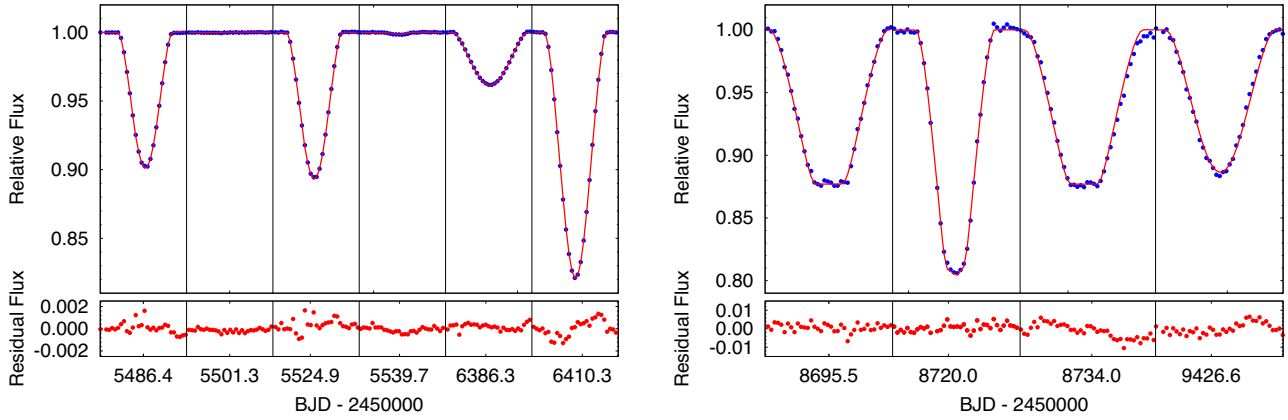


**Figure 4.** Some characteristic primary and secondary eclipses of KIC 5653126 in the *Kepler* (left) and *TESS* light curves (right) overplotted with the photodynamical model solution. All the strips have durations of 0.6 and 0.8 d in the left-hand and right-hand panels, respectively. The left-hand panel shows that between the two consecutive primary eclipses around BJDs 2455486.3 and 2455524.9 no secondary eclipse can be detected, but just one orbital period later, the very first extremely shallow secondary eclipse occurs at ∼2455539.7. The last secondary and primary eclipses observed by *Kepler* are also plotted in the last two segments of the left-hand panel. As one can see, by that time, the durations of the secondary eclipses exceeded that of the primary ones, which is a consequence of the slower orbital motion closer to apastron. In the right-hand panel, all the eclipses (three secondary and one primary minima) observed with *TESS* are plotted. Note, the secondary eclipses in sectors 14 and 15 are clearly flat-bottomed, implying total eclipses, while the S41 secondary eclipse was, again, V-shaped, i.e. a partial eclipse.

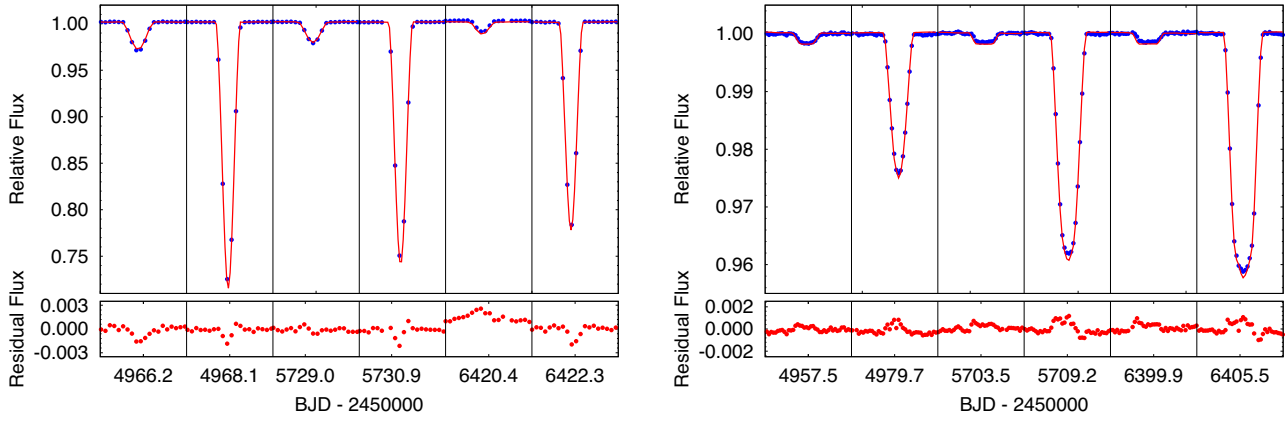


**Figure 5.** Secondary and primary eclipses of KICs 5731312 (left) and 8023317 (right) at the beginning, middle, and end of the 4-yr-long *Kepler* observations. The lengths of the light-curve sections are 0.4 and 0.8 d in the left-hand and right-hand panels, respectively.

*KIC 8023317 = KOI-6049* ($P_1 = 16.58$ d; $P_2 = 611$ d; $P_2/P_1 = 36.9$) displays slowly and continuously increasing primary eclipse depths throughout the $Q0 - Q17$ *Kepler* LC data. (SC data were also gathered during quarters $Q5.2$ and $Q17.1$.) The very shallow secondary eclipses, however, have constant depths during the 4-yr-long data set (see lower-right panel of Fig. 1 and right-hand panel of Fig. 5). This is due to the fact that the flat bottom of the secondary eclipses clearly indicates that during these events, the smaller fainter and colder secondary star was totally eclipsed. The EDV for the first time was reported by Rappaport et al. (2013) who also made the first ETV analysis of the system. The system was also included in the more sophistical ETV analyses of Borkovits et al. (2015, 2016). All three investigations led to similar results, indicating that KIC 8023317 is one of the most inclined triple systems with $i_{\rm mut} = 49\overset{\circ}{.}5 \pm 0\overset{\circ}{.}6$ amongst the EBs observed with *Kepler*. Moreover, similar to KIC 5731312, the analytic solutions of Borkovits et al. (2015, 2016) led to the conclusion that the apsidal motion of this EB is, again, retrograde. This triple was reobserved with *TESS* during sectors 14, 40, and 41. These data exhibit five additional, U-shaped primary eclipses, however, the much smaller signal-to-noise ratio of the *TESS* light curves does not allow for a secure detection of the very low-amplitude secondary eclipses.

## 3 OBSERVATIONAL DATA AND ITS PREPARATION

Our analysis is primarily based on the photometric data gathered by the *Kepler* spacecraft during its 4-yr-long primary mission. We use exclusively the same LC (time resolution of 29.4 min) data sets, which were used in our previous work on the comprehensive ETV analyses of hundreds of *Kepler* EBs (Borkovits et al. 2016). The majority of these light curves were downloaded from the Villanova website[7] of the third revision of the Kepler Eclipsing Binary Catalog (Abdul-Masih et al. 2016; Kirk et al. 2016) while in the case of

[7] http://keplerebs.villanova.edu/

KIC 5731312, the missing quarters 12 and 13 were downloaded directly from the MAST database.[8]

Regarding the more recent *TESS* observations, as mentioned above, all four systems were measured in 30-min cadence mode during Year 2 observations. Additionally, three of the systems (with the exception being KIC 6964043) were also observed in the 10-min cadence mode during the first sectors of Year 4 observations. We processed the original *TESS* FFIs using a convolution-based differential photometric pipeline implemented in the FITSH package (Pál 2012). These raw light curves, however, exhibited large amounts of scattered light and, moreover, due to the large pixel size of *TESS*, the signal of KIC 5653126 was blended with that of the 4.81-d-period EB KIC 5738698 and, therefore, needed disentanglement. This disentanglement was carried out with a principal component analysis (PCA) as follows.

We used the built-in routines from the LIGHTKURVE Python package (Lightkurve Collaboration 2018). First, differential images centred on our targets were constructed by the previously mentioned FITSH pipeline subtracting a median image from the raw images. These differential images were then read in as a 60 × 60 pixel-sized *TargetPixelFile* object and the raw differential light curve was calculated by summing up the residual fluxes in a 3 × 3 pixel-sized aperture around the target. After that, assuming that all of the signal originated from our target is located inside the chosen aperture, all the other pixels outside this aperture were used to constrain a *DesignMatrix* object with the vectors that contain information about scattered light, spacecraft motion, and other leftover extrinsic light variabilities (e.g. the signal of a close variable star partly measured in the aperture). From this *DesignMatrix*, we supplied the first 5–7 principal components to LIGHKURVE's *RegressionCorrector* in order to construct the noise model and remove the underlying systematic noise from the raw light curves, and, in the case of KIC 5653126, also to deblend the signal of KIC 5738698 from the light curve. As a final step, the relative fluxes of the detrended light curves were referenced to the zero-point values calculated from the $G_{\rm RP}$ magnitudes[9] and were normalized to unity.

Moreover, in the case of KIC 5731312, we included in the analysis two additional primary eclipses that were observed by us at Baja Astronomical Observatory (Hungary) between the Year 2 and Year 4 *TESS* observations.

In preparing these data sets for the photodynamical analyses, first we determined accurate eclipse times from the *TESS* and ground-based follow-up observations in the same manner as the *Kepler*-observed eclipse times were determined earlier for our previous analytic ETV analyses in Borkovits et al. (2016). Thus, we obtained 4 (1 primary and 3 secondary) new mid-eclipse times for KIC 5653126 and, moreover, 11 and 5 primary eclipse times for KICs 5731312 and 8023317, respectively. In the case of KIC 6964043, no further eclipses were detected in the *TESS* data. We list all of these eclipse times together with the former *Kepler* data in the tables of Appendix B. Moreover, the ETV curves, together with the best photodynamical fits (see below, in Section 4), are plotted in Fig. 6.

For the photodynamical analysis, we took some additional preparatory steps with the light curves. First, to obtain a more uniform sampling, we converted the Year 4 10-min cadence *TESS* data into 30-min bins. Secondly, in order to save computational time and also to give the eclipses themselves (which carry the vast bulk of both the relevant astrophysical and dynamical information) a higher statistical weight, we kept only small sections of the light curves around the primary and secondary eclipses of the inner binaries. (Note, more strictly speaking, we kept the small sections of the light curves around the minima of the sky-projected distances of the stellar discs of the inner binaries, irrespective of whether eclipses have actually occurred or not.) Moreover, in the case of KIC 6964043, we kept some additional few-day-long sections around the third-body eclipses, as well.

Finally, we note that the light curves also exhibit some low-level systematics, which might have either an instrumental origin or be caused by stellar variability. Due to their very low amplitude, we did not attempt to remove these effects. However, in the future, analyses using a simultaneous fit of Gaussian Processes or wavelet-based (Csizmadia et al. 2021) noise models can remove some of these systematic behaviours and thereby slightly improve the fit and error estimations.

## 4 PHOTODYNAMICAL MODELLING

For the four triple systems, we have carried out a photodynamical analysis with the software package LIGHTCURVEFACTORY (see e.g. Borkovits et al. 2019a, 2020a, and references therein). As described in these earlier papers, the code contains (i) a built-in numerical integrator to calculate the gravitationally (three- or four-body effects), tidally, and (optionally) relativistically perturbed coordinates and velocities of the three (four) stars in the system; (ii) emulators for multiband light curves (allowing multiple eclipses), ETV curves, and radial velocity (RV) curves (if available), (iii) built-in, tabulated PARSEC grids (Bressan et al. 2012) for interpolating fundamental stellar parameters (e.g. radii and effective temperatures), as well as composite spectral energy distribution (SED) model for the three (four) stars, and (iv) a Markov chain Monte Carlo (MCMC-) based search routine for fitting the parameters. The latter utilizes an implementation of the generic Metropolis-Hastings algorithm (see e.g. Ford 2005). The use of this software package and the consecutive steps of the entire analysis process have been previously explained in detail as the code was applied to a variety of multiple stellar systems (Borkovits et al. 2018, 2019a, b, 2020a, b, 2021, 2022; Mitnyan et al. 2020; Rappaport et al. 2022).

For the four current systems, in the absence of RV data, we combined a composite SED analysis and the use of precalculated PARSEC grids as proxies to determine the masses of the constituent stars. As a consequence, such a photodynamical model solution is no longer astrophysically model-independent. None the less, in our previous work (Borkovits et al. 2022), we have shown that for compact, strongly dynamically interacting triples (as is the case for the currently investigated systems), such a solution (which we call 'MDN' – astrophysical model-dependent solution without RV data) results in fundamental stellar parameters (masses, radii) within 5–10 per cent to the results of an 'MIR' (astrophysical model-independent solution with RV data) solution. The geometric and dynamical parameters (i.e. the orbital elements and, also the mass ratios), as well as dimensionless quantities like the fractional radii and temperature ratios of the stars, remain practically unchanged between the MDN and MIR solutions.

In the case of these 'MDN' runs, the adjusted parameters were as follows:

(i) Orbits: Three of six orbital-element related parameters of the inner, and six parameters of the outer orbits, i.e. the components of the eccentricity vectors of both orbits $(e\sin\omega)_{\rm in,\,out}$, $(e\cos\omega)_{\rm in,\,out}$, the

[8] https://archive.stsci.edu/missions-and-data/kepler

[9] This is a rather good approximation due to the significant overlap between the passbands of *TESS* and *Gaia* (Ricker et al. 2015; Jordi et al. 2010)

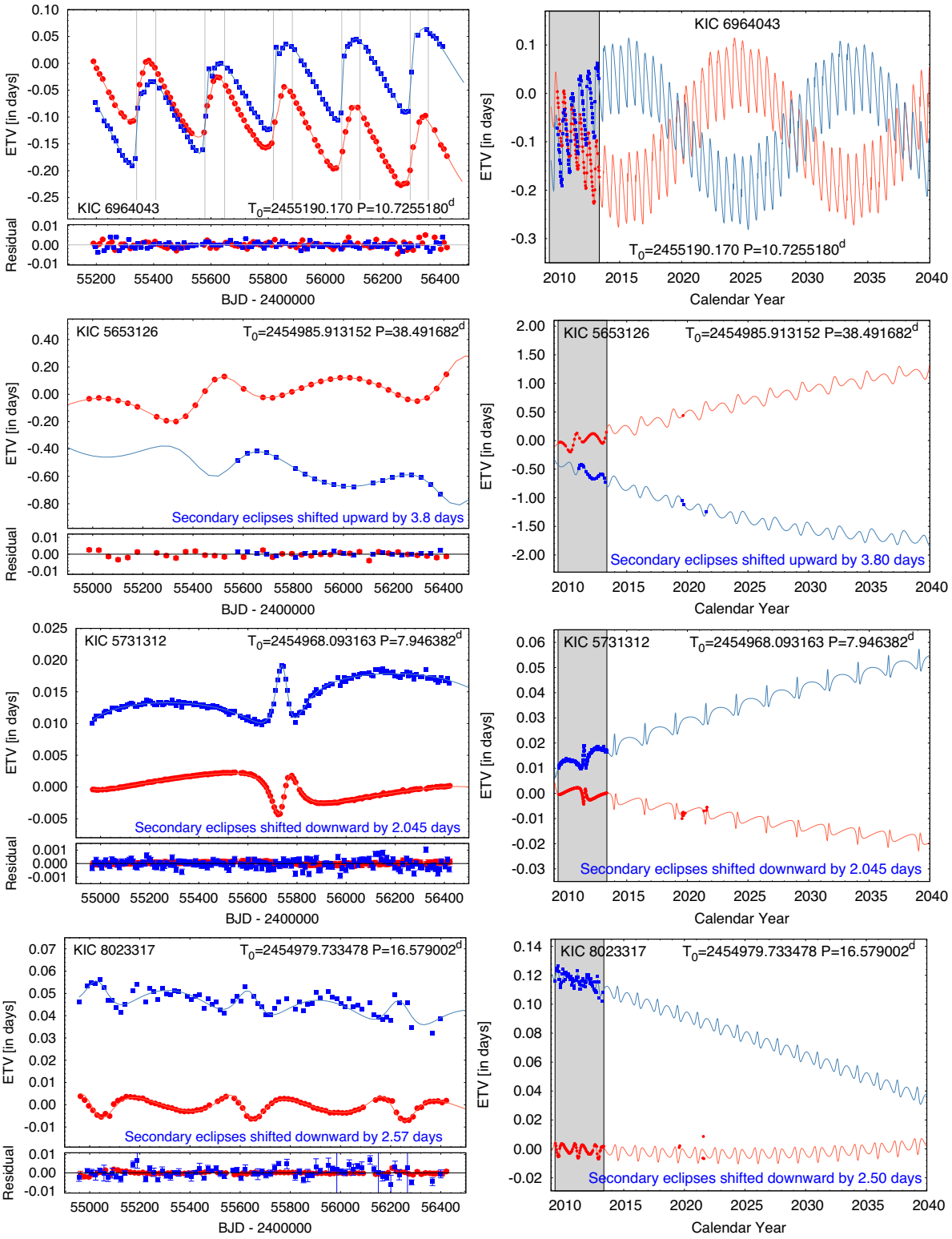


**Figure 6.** ETVs of KICs 6964043 (upper), 5653126 (second row), 5731312 (third row), and 8023317 (bottom). Left-hand panels represent the timing variations during the *Kepler* observations, while right-hand panels exhibit longer time intervals up to 2040. In these panels, grey-shaded area shows the nominal interval of the original *Kepler* mission. (Note, in those parts of the curves, where no eclipses would be observed due to the low orbital inclinations, the times of the minimal sky-projected distances of the stellar discs were calculated.) Red and blue dots represent the primary and secondary binary eclipses, respectively, while the correspondingly coloured curves connect the best-fitting photodynamical model ETV points. In the upper-left panel, the solid vertical grey lines indicate the times of the third-body eclipses detected by *Kepler* in the triple system KIC 6964043. The lower parts of the left-hand panels show the residuals from the model fit.

inclinations relative to the plane of the sky ($i_{\rm in,\,out}$), and moreover, three other parameters for the outer orbit, including the period ($P_{\rm out}$), the longitude of the node relative to the inner binary's node ($\Omega_{\rm out}$), and, in the case of the triply eclipsing system KIC 6964043, the sixth parameter was the time of the first (inferior) conjunction of the tertiary star observed in the *Kepler* data ($\mathcal{T}^{\rm inf}_{\rm out}$) (which corresponds to the first observed third-body eclipse), while for the other three systems the periastron passage times ($\tau_{\rm out}$) were adjusted.

(ii) Stars: Three stellar mass-related parameters: the mass of the most massive component (being either $m_{\rm Aa}$, the primary of the inner pair or, $m_{\rm B}$, the tertiary star), and the inner and outer mass ratios ($q_{\rm in,\,out}$). Additionally, the metallicity of the system ([*M*/*H*]), the (logarithmic) age of the three coeval stars ($\log\tau$), and the interstellar reddening $E(B-V)$ towards the given triple were also varied. Moreover, due to the strong contamination of the *TESS* light curve of KIC 8023317, for this light curve only, the 'extra light' contamination, $\ell_4$ parameter was also freely adjusted.

A couple of other parameters were *constrained* instead of being adjusted or held constant during our analyses, as follows:

(i) Orbits: The orbital period of the inner binary ($P_{\rm in}$) and its orbital phase (through the time of an arbitrary primary eclipse or, more strictly, the time of the inferior conjunction of the secondary star – $\mathcal{T}^{\rm inf}_{\rm in}$) were constrained internally through the ETV curves.

(ii) Stars: The radii and temperatures of the three stars were calculated with the use of three-linear interpolations from the precomputed 3D (metallicity; logarithmic age; stellar mass) PARSEC grids. Additionally, the distance of the system (which is necessary for the SED fitting) were calculated *a posteriori* at the end of each trial step, by minimizing the value of $\chi^2_{\rm SED}$.

(iii) Atmospheric parameters of the stars: we handled them in a similar manner as in our previous photodynamical studies. We utilized a logarithmic limb-darkening law (Klinglesmith & Sobieski 1970) for which the passband-dependent linear and non-linear coefficients were interpolated in each trial step via the tables from the original version of the Phoebe software (Prša & Zwitter 2005). We set the gravity darkening exponents for all late type stars to $\beta = 0.32$ in accordance with the classic model of Lucy (1967) valid for convective stars and held them constant. Note, however, that the choice of this parameter has only minor consequences, since the stars in the present study are close to spheroids.

The median values of the orbital and physical parameters, as well as some derived quantities, of the four triple systems, computed from the MCMC posteriors and their $1\sigma$ uncertainties are tabulated in Tables 2 and 3. Furthermore, the observed versus model light curves are plotted in Figs 1–5, while the observed versus model ETV curves are shown in Fig. 6.

## 5 DISCUSSION

In this section, first we briefly describe the photodynamical results for each individual system, and then we study the short and longer term dynamical evolutions of our triples. For the investigation of the short- and long-term dynamical evolutions, we integrate the future motion of the triple star systems with two different numerical integrators. For the short-term ($\leq$1 Myr-long) integration, we use the very same integrator which is built into LIGHTCURVEFACTORY, and described in Borkovits et al. (2019a, b). Here, we note that this integrator works directly with the equations of the orbital motions, including point-mass, tidal, and relativistic contributions, and the Eulerian equations of uni-axial stellar rotations. Its main advantage is that it returns at every integration step the spatial coordinates and velocities of each star and, therefore, can be used directly to generate the system light curve. It also gives the osculating orbital elements at each instant and, hence, the observational consequences of the motions can be easily studied. The disadvantages are, however, that neither stellar evolution nor tidal dissipation are built in and, therefore, it cannot be used for realistic simulations on much longer time-scales. Moreover, another disadvantage is that it is much slower than the method we use for the investigations of the long-term (up to several Gyrs) dynamical evolution of the systems. For this latter approach we use the triple stellar evolution code *TRES* (Toonen, Hamers & Portegies Zwart 2016), which incorporates secular dynamical evolution, including the quadrupole & octupole level interactions, stellar evolution including stellar winds & stellar interaction processes, such as mass transfer, common-envelope (CE) evolution, mergers, tidal forces, and gravitational wave emission.[10]

Finally, we discuss the implications of our findings on the system parameters for the formation processes of multiple stellar systems in general.

### 5.1 KIC 69640403

This is the only triply eclipsing triple among our sample, and the system is found to be nearly flat. In contrast to the previous findings of Borkovits et al. (2015, 2016), here we find the mutual inclination of the inner and outer orbital planes to be $i_{\rm mut} = 4\overset{\circ}{.}14 \pm 0\overset{\circ}{.}09$. This is also the only system in the present study for which the outer stellar component was found to be the most massive one. This tertiary is a slightly evolved twin of our Sun ($m_{\rm B} = 1.00 \pm 0.08\,{\rm M}_\odot$; $R_{\rm B} = 1.98 \pm 0.09\,{\rm R}_\odot$; $T_{\rm eff,B} = 5500 \pm 50$ K), and it emits more than 96 per cent of the total flux of the system (at least in the *Kepler* photometric band). The inner binary consists of two very similar red dwarf stars ($m_{\rm Aa} = 0.59 \pm 0.04\,{\rm M}_\odot$; $R_{\rm Aa} = 0.59 \pm 0.03\,{\rm R}_\odot$; $T_{\rm eff,Aa} = 4130 \pm 50$ K and $m_{\rm Ab} = 0.57 \pm 0.04\,{\rm M}_\odot$; $R_{\rm Ab} = 0.57 \pm 0.03\,{\rm R}_\odot$; $T_{\rm eff,Ab} = 4040 \pm 40$ K, respectively). This triple was found to be the oldest ($\tau = 9^{+1}_{-2}$ Gyr) and most distant ($d = 2450 \pm 120$ pc) among the set of studied systems. The distance is greater by $\approx 2\sigma$ than the Gaia EDR3 distance, but such an inconsistency, in the case of a triple system with an outer period near 2/3 of a year, might be expected. Both the inner and outer mass ratios are relatively close to unity ($q_{\rm in} = 0.97 \pm 0.01$ and $q_{\rm out} = 0.87 \pm 0.01$) which, together with the flatness and compact nature of the system, imply that this system might have formed through a sequential disc instability mechanism (Tokovinin & Moe 2020; Tokovinin 2021), which may lead to compact triple systems with both the inner and outer mass ratios close to unity (double twins, Tokovinin 2018).

Regarding the orbital parameters, while the inner orbit is only slightly eccentric ($e_{\rm in} = 0.0037 \pm 0.0005$), the eccentricity of the outer orbit is moderately high ($e_{\rm out} = 0.4781 \pm 0.0006$). As a consequence, the periastron distance of the outer orbit is $a_{\rm out}(1-e_{\rm out}) \approx 5.1\,a_{\rm in}$, which places the system quite close to the dynamical stability limit; however, the system is definitely within the dynamically stable region. This is clearly illustrated in the upper panels of Fig. 7, which show the variations of the inner eccentricity and the mutual inclination over the first 250 yr of our 1 million

[10]Note, we have also numerically integrated the dynamical evolution of the systems with *TRES* on the shorter time-scales and obtained similar (dynamical) results to those found with the built in integrator of LIGHTCURVEFACTORY for all four systems considered in this paper.

**Table 2.** Orbital and astrophysical parameters of the low mutual inclination triples KICs 6964043 and 5653126 from the joint photodynamical light curve, ETV, SED, and PARSEC isochrone solution. Note, besides the usual angular orbital elements (given in both the observational and dynamical frame of references), $i_{\rm inv}$ and $\Omega_{\rm inv}$ give the position of the invariable plane with respect to the tangential plane of the sky. The osculating orbital elements are given for epochs $t_0$, given in the first row.

| | KIC 6964043 | | KIC 5653126 | |
|---|---|---|---|---|
| | Orbital elements | | | |
| | Aa–Ab | A–B | Aa–Ab | A–B |
| $t_0$ (BJD - 2400000) | 55182.0 | | 54953.0 | |
| $P$ (d) | $10.69787^{+0.00012}_{-0.00015}$ | $239.2519^{+0.0076}_{-0.0083}$ | $38.44825^{+0.00028}_{-0.00028}$ | $971.39^{+0.25}_{-0.25}$ |
| $a$ [$R_\odot$) | $21.47^{+0.47}_{-0.34}$ | $209.8^{+4.9}_{-3.6}$ | $69.77^{+0.26}_{-0.35}$ | $675.8^{+3.0}_{-3.8}$ |
| $e$ | $0.03687^{+0.00025}_{-0.00052}$ | $0.47806^{+0.00056}_{-0.00053}$ | $0.2935^{+0.0015}_{-0.0021}$ | $0.1787^{+0.0011}_{-0.0011}$ |
| $\omega$ (deg) | $75.46^{+0.15}_{-0.15}$ | $311.41^{+0.09}_{-0.10}$ | $304.36^{+0.32}_{-0.22}$ | $323.90^{+0.36}_{-0.32}$ |
| $i$ (deg) | $88.797^{+0.111}_{-0.087}$ | $89.811^{+0.013}_{-0.015}$ | $87.128^{+0.018}_{-0.018}$ | $87.608^{+0.526}_{-0.463}$ |
| $\mathcal{T}_0^{\rm inf}$ (BJD - 2400000) | $55190.1678^{+0.0004}_{-0.0004}$ | $55340.658^{+0.018}_{-0.015}$ | $54985.8390.1678^{+0.0007}_{-0.0007}$ | ... |
| $\tau$ (BJD - 2400000) | $55184.3510^{+0.0043}_{-0.0044}$ | $55110.444^{+0.047}_{-0.050}$ | $54949.355^{+0.030}_{-0.020}$ | $55481.39^{+0.65}_{-0.63}$ |
| $\Omega$ (deg) | 0.0 | $-4.023^{+0.089}_{-0.086}$ | 0.0 | $-12.344^{+0.163}_{-0.175}$ |
| $i_{\rm mut}$ (deg) | $4.138^{+0.087}_{-0.061}$ | | $12.348^{+0.168}_{-0.152}$ | |
| $\omega^{\rm dyn}$ (deg) | $331.3^{+1.7}_{-1.3}$ | $27.2^{+1.8}_{-1.4}$ | $212.4^{+2.0}_{-2.1}$ | $51.3^{+2.1}_{-2.1}$ |
| $i^{\rm dyn}$ (deg) | $3.620^{+0.076}_{-0.055}$ | $0.519^{+0.009}_{-0.008}$ | $10.152^{+0.129}_{-0.119}$ | $2.197^{+0.041}_{-0.036}$ |
| $\Omega^{\rm dyn}$ (deg) | $284.2^{+1.3}_{-1.8}$ | $104.2^{+1.3}_{-1.8}$ | $272.4^{+2.4}_{-2.1}$ | $92.4^{+2.4}_{-2.1}$ |
| $i_{\rm inv}$ (deg) | $89.685^{+0.015}_{-0.017}$ | | $87.514^{+0.437}_{-0.383}$ | |
| $\Omega_{\rm inv}$ (deg) | $-3.506^{+0.045}_{-0.062}$ | | $-10.149^{+0.127}_{-0.135}$ | |
| Mass ratio ($q = m_{\rm sec}/m_{\rm pri}$) | $0.972^{+0.008}_{-0.009}$ | $0.866^{+0.009}_{-0.007}$ | $0.736^{+0.006}_{-0.006}$ | $0.418^{+0.004}_{-0.004}$ |
| $K_{\rm pri}$ (km s$^{-1}$) | $50.06^{+1.10}_{-0.77}$ | $23.41^{+0.74}_{-0.44}$ | $40.69^{+0.22}_{-0.28}$ | $10.52^{+0.11}_{-0.11}$ |
| $K_{\rm sec}$ (km s$^{-1}$) | $51.54^{+1.04}_{-0.70}$ | $27.09^{+0.46}_{-0.37}$ | $55.28^{+0.25}_{-0.37}$ | $25.18^{+0.09}_{-0.09}$ |
| | Apsidal and nodal motion related parameters | | | |
| $P_{\rm apse}$ (yr) | $28.56^{+0.12}_{-0.15}$ | $199.8^{+0.8}_{-0.7}$ | $309^{+3}_{-4}$ | $1204^{+3}_{-4}$ |
| $P_{\rm apse}^{\rm dyn}$ (yr) | $13.34^{+0.05}_{-0.06}$ | $22.21^{+0.06}_{-0.07}$ | $131.4^{+0.9}_{-0.7}$ | $190^{+2}_{-2}$ |
| $P_{\rm node}^{\rm dyn}$ (yr) | $24.99^{+0.10}_{-0.08}$ | | $225^{+3}_{-3}$ | |
| $\Delta\omega_{\rm 3b}$ (arcsec/cycle) | $1329^{+7}_{-6}$ | $4249^{+16}_{-16}$ | $441^{+6}_{-4}$ | $2863^{+10}_{-7}$ |
| $\Delta\omega_{\rm GR}$ (arcsec/cycle) | $0.447^{+0.020}_{-0.014}$ | $0.111^{+0.005}_{-0.004}$ | $0.399^{+0.003}_{-0.004}$ | $0.0553^{+0.0005}_{-0.0006}$ |
| $\Delta\omega_{\rm tide}$ (arcsec/cycle) | $0.026^{+0.005}_{-0.004}$ | ... | $0.050^{+0.001}_{-0.002}$ | ... |
| | stellar parameters | | | |
| | Aa | Ab | B | Aa | Ab | B |
| | Relative quantities | | | | | |
| Fractional radius ($R/a$) | $0.0274^{+0.0008}_{-0.0007}$ | $0.0266^{+0.0010}_{-0.0008}$ | $0.00944^{+0.00022}_{-0.00024}$ | $0.0315^{+0.0002}_{-0.0002}$ | $0.0188^{+0.0002}_{-0.0002}$ | $0.00190^{+0.00004}_{-0.00004}$ |
| Temperature relative to $(T_{\rm eff})_{\rm Aa}$ | 1 | $0.9786^{+0.0069}_{-0.0075}$ | $1.3303^{+0.0175}_{-0.0159}$ | 1 | $0.8877^{+0.0077}_{-0.0042}$ | $0.8824^{+0.0036}_{-0.0035}$ |
| Fractional flux (in *Kepler*-band) | $0.0203^{+0.0012}_{-0.0012}$ | $0.0174^{+0.0010}_{-0.0009}$ | $0.9623^{+0.0017}_{-0.0020}$ | $0.6875^{+0.0098}_{-0.0093}$ | $0.1588^{+0.0048}_{-0.0050}$ | $0.1532^{+0.0073}_{-0.0061}$ |
| Fractional flux (in *TESS*-band) | – | – | – | $0.4995^{+0.01791}_{-0.0165}$ | $0.1227^{+0.0016}_{-0.0016}$ | $0.1084^{+0.0048}_{-0.0050}$ |
| | Physical Quantities | | | | | |
| $m$ ($M_\odot$) | $0.588^{+0.038}_{-0.026}$ | $0.571^{+0.038}_{-0.028}$ | $1.003^{+0.081}_{-0.055}$ | $1.774^{+0.024}_{-0.029}$ | $1.303^{+0.018}_{-0.016}$ | $1.285^{+0.025}_{-0.029}$ |
| $R$ ($R_\odot$) | $0.588^{+0.031}_{-0.025}$ | $0.571^{+0.034}_{-0.027}$ | $1.980^{+0.087}_{-0.077}$ | $2.198^{+0.017}_{-0.017}$ | $1.310^{+0.022}_{-0.020}$ | $1.281^{+0.034}_{-0.037}$ |
| $T_{\rm eff}$ (K) | $4134^{+45}_{-49}$ | $4041^{+44}_{-41}$ | $5495^{+42}_{-45}$ | $7062^{+53}_{-88}$ | $6260^{+59}_{-47}$ | $6228^{+47}_{-64}$ |
| $L_{\rm bol}$ ($L_\odot$) | $0.091^{+0.013}_{-0.010}$ | $0.079^{+0.011}_{-0.010}$ | $3.234^{+0.240}_{-0.279}$ | $10.822^{+0.353}_{-0.626}$ | $2.384^{+0.103}_{-0.132}$ | $2.225^{+0.157}_{-0.201}$ |
| $M_{\rm bol}$ | $7.38^{+0.12}_{-0.14}$ | $7.53^{+0.15}_{-0.14}$ | $3.50^{+0.10}_{-0.08}$ | $2.18^{+0.06}_{-0.03}$ | $3.83^{+0.06}_{-0.05}$ | $3.90^{+0.10}_{-0.07}$ |
| $M_V$ | $8.27^{+0.15}_{-0.14}$ | $8.50^{+0.16}_{-0.12}$ | $3.62^{+0.11}_{-0.08}$ | $2.10^{+0.07}_{-0.03}$ | $3.80^{+0.07}_{-0.05}$ | $3.88^{+0.11}_{-0.08}$ |
| $\log g$ (dex) | $4.668^{+0.018}_{-0.017}$ | $4.679^{+0.022}_{-0.021}$ | $3.846^{+0.016}_{-0.014}$ | $4.000^{+0.007}_{-0.006}$ | $4.317^{+0.009}_{-0.009}$ | $4.331^{+0.016}_{-0.015}$ |
| | Global system parameters | | | | | |
| log (age) (dex) | $9.934^{+0.075}_{-0.107}$ | | | $9.016^{+0.028}_{-0.038}$ | | |
| $[M/H]$ (dex) | $-0.230^{+0.148}_{-0.094}$ | | | $0.372^{+0.059}_{-0.107}$ | | |
| $E(B-V)$ (mag) | $0.088^{+0.015}_{-0.012}$ | | | $0.351^{+0.014}_{-0.026}$ | | |
| Extra light $\ell_4$ (in *TESS*-band) | ... | | | $0.270^{+0.019}_{-0.046}$ | | |
| $(M_V)_{\rm tot}$ | $3.59^{+0.11}_{-0.08}$ | | | $1.73^{+0.07}_{-0.03}$ | | |
| Distance (pc) | $2443^{+119}_{-109}$ | | | $1374^{+16}_{-14}$ | | |

**Table 3.** The same as in Table 2 but for KICs 5731312 and 8023317.

| | KIC 5731312 | | KIC 8023317 | |
|---|---|---|---|---|
| | Orbital elements | | | |
| | Aa–Ab | A–B | Aa–Ab | A–B |
| $t_0$ (BJD - 2400000) | 54953.0 | | 54953.0 | |
| $P$ (d) | $7.946521^{+0.000011}_{-0.000010}$ | $917.00^{+0.98}_{-0.92}$ | $16.57544^{+0.00021}_{-0.00020}$ | $605.4^{+2.3}_{-2.2}$ |
| $a$ ($R_\odot$) | $18.20^{+0.10}_{-0.09}$ | $448.0^{+2.5}_{-2.1}$ | $32.63^{+0.45}_{-0.42}$ | $368.1^{+5.5}_{-4.4}$ |
| $e$ | $0.45866^{+0.00048}_{-0.00033}$ | $0.5745^{+0.0077}_{-0.0079}$ | $0.27889^{+0.00041}_{-0.00068}$ | $0.252^{+0.013}_{-0.013}$ |
| $\omega$ (deg) | $206.82^{+0.15}_{-0.12}$ | $36.06^{+1.38}_{-1.59}$ | $152.90^{+0.32}_{-0.15}$ | $159.14^{+2.91}_{-2.66}$ |
| $i$ (deg) | $87.378^{+0.153}_{-0.107}$ | $67.649^{+0.487}_{-0.354}$ | $87.019^{+0.045}_{-0.046}$ | $71.836^{+0.369}_{-0.267}$ |
| $\mathcal{T}_0^{\rm inf}$ (BJD - 2400000) | $54968.0942^{+0.0002}_{-0.0002}$ | ... | $54979.7311^{+0.0003}_{-0.0003}$ | – |
| $\tau$ (BJD - 2400000) | $54967.5686^{+0.0023}_{-0.0017}$ | $54830.70^{+1.70}_{-1.97}$ | $54975.7719^{+0.0135}_{-0.0061}$ | $55023.12^{+4.82}_{-4.22}$ |
| $\Omega$ (deg) | 0.0 | $35.18^{+0.41}_{-0.43}$ | 0.0 | $-55.25^{+0.86}_{-0.81}$ |
| $i_{\rm mut}$ (deg) | $39.41^{+0.32}_{-0.31}$ | | $55.71^{+0.79}_{-0.82}$ | |
| $\omega^{\rm dyn}$ (deg) | $263.9^{+0.5}_{-0.6}$ | $281.1^{+1.5}_{-1.7}$ | $79.4^{+0.4}_{-0.3}$ | $255.9^{+2.7}_{-2.6}$ |
| $i^{\rm dyn}$ (deg) | $27.20^{+0.33}_{-0.34}$ | $12.22^{+0.37}_{-0.37}$ | $33.38^{+0.85}_{-0.88}$ | $22.33^{+0.52}_{-0.53}$ |
| $\Omega^{\rm dyn}$ (deg) | $118.9^{+0.6}_{-0.6}$ | $298.9^{+0.6}_{-0.6}$ | $257.9^{+0.5}_{-0.4}$ | $77.9^{+0.5}_{-0.4}$ |
| $i_{\rm inv}$ (deg) | $73.22^{+0.23}_{-0.24}$ | | $78.59^{+0.28}_{-0.21}$ | |
| $\Omega_{\rm inv}$ (deg) | $23.62^{+0.39}_{-0.39}$ | | $-32.62^{+0.90}_{-0.84}$ | |
| mass ratio ($q = m_{\rm sec}/m_{\rm pri}$) | $0.665^{+0.031}_{-0.042}$ | $0.120^{+0.004}_{-0.004}$ | $0.303^{+0.010}_{-0.013}$ | $0.079^{+0.003}_{-0.003}$ |
| $K_{\rm pri}$ (km s$^{-1}$) | $52.05^{+1.63}_{-2.28}$ | $2.99^{+0.08}_{-0.08}$ | $23.99^{+0.48}_{-0.50}$ | $2.25^{+0.07}_{-0.07}$ |
| $K_{\rm sec}$ (km s$^{-1}$) | $78.48^{+1.50}_{-1.40}$ | $24.96^{+0.20}_{-0.21}$ | $79.45^{+2.15}_{-1.56}$ | $28.51^{+0.34}_{-0.46}$ |
| | Apsidal motion related parameters | | | |
| $P_{\rm apse}$ (yr) | $-4787^{+280}_{-306}$ | $18193^{+1368}_{-1238}$ | $-653^{+31}_{-36}$ | $-6567^{+676}_{-929}$ |
| $P_{\rm apse}^{\rm dyn}$ (yr) | $1298^{+34}_{-33}$ | $873^{+18}_{-18}$ | $-1707^{+229}_{-342}$ | $1103^{+56}_{-54}$ |
| $P_{\rm node}^{\rm dyn}$ (yr) | $899^{+18}_{-18}$ | | $884^{+24}_{-23}$ | |
| $\Delta\omega_{\rm 3b}$ (arcsec/cycle) | $-7.1^{+0.3}_{-0.4}$ | $179^{+13}_{-13}$ | $-91^{+5}_{-5}$ | $-327^{+41}_{-38}$ |
| $\Delta\omega_{\rm GR}$ (arcsec/cycle) | $0.736^{+0.008}_{-0.007}$ | $0.0395^{+0.0005}_{-0.0005}$ | $0.465^{+0.013}_{-0.012}$ | $0.044^{+0.001}_{-0.001}$ |
| $\Delta\omega_{\rm tide}$ (arcsec/cycle) | $0.47^{+0.02}_{-0.02}$ | ... | $0.516^{+0.034}_{-0.035}$ | ... |
| | stellar parameters | | | |
| | Aa | Ab | B | Aa | Ab | B |
| | Relative quantities | | | | | |
| Fractional radius ($R/a$) | $0.0399^{+0.0007}_{-0.0005}$ | $0.0277^{+0.0011}_{-0.0015}$ | $0.000409^{+0.000009}_{-0.000009}$ | $0.0600^{+0.0007}_{-0.0007}$ | $0.0121^{+0.0002}_{-0.0002}$ | $0.000474^{+0.000017}_{-0.000015}$ |
| Temperature relative to $(T_{\rm eff})_{\rm Aa}$ | 1 | $0.7272^{+0.0189}_{-0.0225}$ | $0.5733^{+0.0058}_{-0.0053}$ | 1 | $0.5402^{+0.0056}_{-0.0061}$ | $0.4393^{+0.0056}_{-0.0063}$ |
| Fractional flux (in *Kepler*-band) | $0.8986^{+0.0207}_{-0.0202}$ | $0.0984^{+0.0200}_{-0.0208}$ | $0.0031^{+0.0003}_{-0.0003}$ | $0.9978^{+0.0001}_{-0.0002}$ | $0.0021^{+0.0002}_{-0.0001}$ | $0.0001^{+0.00001}_{-0.00001}$ |
| Fractional flux (in *TESS*-band) | $0.8774^{+0.0233}_{-0.0220}$ | $0.1194^{+0.0218}_{-0.0233}$ | $0.0033^{+0.0003}_{-0.0003}$ | $0.8479^{+0.0256}_{-0.0177}$ | $0.0023^{+0.0002}_{-0.0002}$ | $0.0001^{+0.00001}_{-0.00001}$ |
| Fractional flux (in $r$'-band) | $0.9086^{+0.0197}_{-0.0193}$ | $0.0892^{+0.0192}_{-0.0198}$ | $0.0022^{+0.0002}_{-0.0002}$ | ... | ... | ... |
| | Physical Quantities | | | | | |
| $m$ ($M_\odot$) | $0.773^{+0.008}_{-0.013}$ | $0.510^{+0.022}_{-0.026}$ | $0.153^{+0.004}_{-0.005}$ | $1.300^{+0.071}_{-0.058}$ | $0.392^{+0.008}_{-0.009}$ | $0.134^{+0.006}_{-0.006}$ |
| $R$ ($R_\odot$) | $0.728^{+0.009}_{-0.009}$ | $0.505^{+0.023}_{-0.029}$ | $0.184^{+0.004}_{-0.004}$ | $1.963^{+0.029}_{-0.046}$ | $0.394^{+0.008}_{-0.010}$ | $0.174^{+0.008}_{-0.007}$ |
| $T_{\rm eff}$ (K) | $5079^{+47}_{-56}$ | $3693^{+68}_{-91}$ | $2911^{+28}_{-26}$ | $5869^{+66}_{-73}$ | $3166^{+45}_{-42}$ | $2575^{+35}_{-36}$ |
| $L_{\rm bol}$ ($L_\odot$] | $0.316^{+0.020}_{-0.018}$ | $0.042^{+0.008}_{-0.008}$ | $0.0022^{+0.0002}_{-0.0002}$ | $4.084^{+0.196}_{-0.215}$ | $0.014^{+0.001}_{-0.001}$ | $0.0012^{+0.0001}_{-0.0001}$ |
| $M_{\rm bol}$ | $6.02^{+0.06}_{-0.07}$ | $8.20^{+0.23}_{-0.18}$ | $11.43^{+0.08}_{-0.08}$ | $3.24^{+0.06}_{-0.05}$ | $9.41^{+0.06}_{-0.06}$ | $12.07^{+0.11}_{-0.12}$ |
| $M_V$ | $6.27^{+0.09}_{-0.08}$ | $9.56^{+0.36}_{-0.26}$ | $14.68^{+0.19}_{-0.19}$ | $3.27^{+0.07}_{-0.06}$ | $11.91^{+0.18}_{-0.20}$ | $16.72^{+0.15}_{-0.17}$ |
| log $g$ (dex) | $4.599^{+0.007}_{-0.006}$ | $4.739^{+0.027}_{-0.021}$ | $5.095^{+0.007}_{-0.007}$ | $3.967^{+0.013}_{-0.011}$ | $4.839^{+0.013}_{-0.009}$ | $5.077^{+0.021}_{-0.020}$ |
| | Global system parameters | | | | | |
| log (age) (dex) | $9.775^{+0.043}_{-0.046}$ | | | $9.639^{+0.036}_{-0.064}$ | | |
| [$M$/$H$] (dex) | $-0.122^{+0.027}_{-0.040}$ | | | $0.330^{+0.064}_{-0.150}$ | | |
| $E(B-V)$ (mag) | $0.038^{+0.009}_{-0.011}$ | | | $0.080^{+0.026}_{-0.019}$ | | |
| Extra light $\ell_4$ (in *TESS*-band) | ... | | | $0.150^{+0.018}_{-0.026}$ | | |
| $(M_V)_{\rm tot}$ | $6.22^{+0.08}_{-0.07}$ | | | $3.27^{+0.07}_{-0.06}$ | | |
| Distance (pc) | $353^{+6}_{-7}$ | | | $814^{+13}_{-22}$ | | |

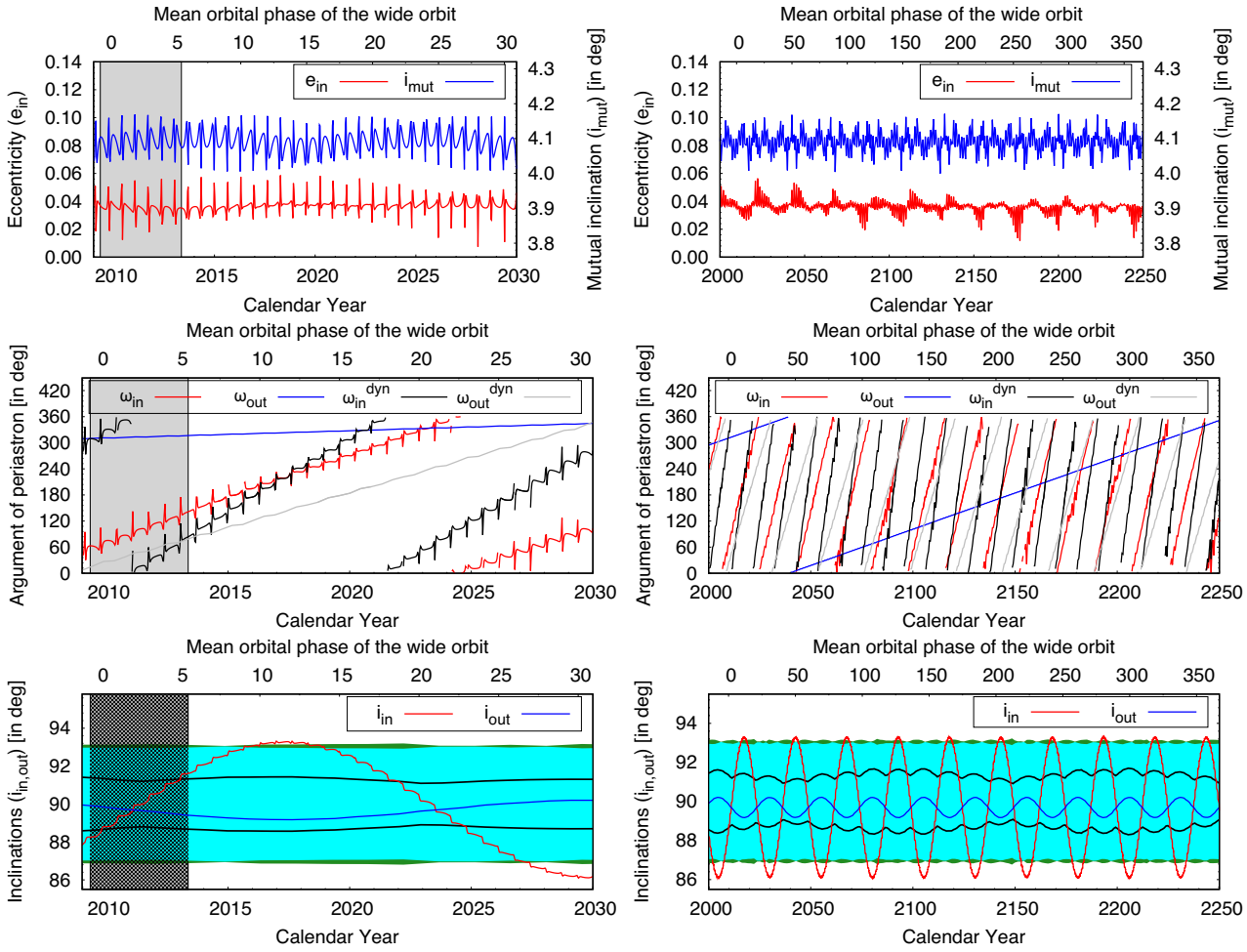


**Figure 7.** Variations of some of the osculating orbital elements in the triple system KIC 6964043. The left-hand panels represent short time-scale variations from 2009 to 2030, while the right-hand panels show 250 yr. The vertical shaded area in the left-hand panels denote the time domain of the original *Kepler* mission. Note, that the medium-period perturbation effects, especially the bumps around the periastron passages of the third component, are also nicely visible on the left-hand panels. *Upper panels:* variations of the inner eccentricity ($e_{in}$) and the mutual inclination ($i_{mut}$). *Middle panels:* the variations of the observable and dynamical arguments of periastrons of the inner and outer orbits ($\omega_{in,\,out}$ and $\omega^{dyn}_{in,out}$, respectively). *Lower panels:* variations of the observable inclinations of the inner and outer orbital planes ($i_{in}$, $i_{out}$, respectively). The green area represents the domain where at least one of the inner EB's eclipses should be observed, while the cyan area stands for the inclination domain where both eclipses can be observed. Moreover, the horizontal black lines stand for the upper and lower outer inclination ($i_{out}$) limits of the domain where outer, third-body eclipses might occur. See text for further details.

yr-long numerical integration. This short-term stability is mainly guaranteed by the nearly perfect flatness of the system, which leads to the suppression of any long-term or secular perturbations in the semimajor axes, as well as to the almost complete disappearance of the quadrupole order long-term perturbations in the eccentricities and the mutual inclination. Moreover, due to the nearly equal masses of the inner binary, the octupole-order terms also remain very small.

In the middle and bottom panels of Fig. 7, we show decades-long (left) and centuries-long (right) variations of some further orbital elements, which have readily detectable observational consequences. In the middle panels, the time evolution of the observational and dynamical arguments of periastrons ($\omega_{in,\,out}$ and $\omega^{dyn}_{in,out}$, respectively) are shown. Similar to the other three triples, the apsidal advances of both the inner and outer orbits are clearly dominated by third-body perturbations over the relativistic and tidal effects (see the corresponding rows in Table 2). Due to the flatness of the system, again the apsidal motion is practically linear in time, apart from the small amplitude $P_{out}$-medium period time-scale variations. The theoretical[11] inner and outer apsidal motion periods in the dynamical frame are $P^{dyn}_{apse} = 13$ and 199 yr, respectively. Naturally, in the observational frame, a much longer apsidal motion period will be observed due to the counterbalancing effect of the nodal regression.[12] Thus, the apsidal motion of the inner binary in the observational frame of reference, which can be detected directly through the anticorrelated primary and secondary ETV curves (Fig. 6), has a

[11]For the calculations, we used the formulae described in Borkovits et al. (2015), appendix C.

[12]It can be readily shown that the observable and dynamical apsidal motion rates relate to each other as $\Delta\omega = \Delta\omega^{dyn} + \Delta\Omega^{dyn}\cos i_{dyn} - \Delta\Omega\cos i$ (see e.g. Borkovits, Forgács-Dajka & Regály 2007; Borkovits et al. 2015). For EBs $\cos i \ll 1$ hence, the last term is negligible (though it was taken into account for calculating the theoretical observable apsidal motion periods – $P_{apse}$, tabulated in Tables 2 and 3) and therefore, for the negative sign of $\Delta\Omega^{dyn}$, one can infer that the observable apsidal advance rate should be lower than the dynamical one.

theoretical period of $P_{\rm apse} = 28.59 \pm 0.02$ yr, in accord with both the numerical integrations and the observed ETV curves.

The bottom panels of Fig. 7 display the inclination angle variations of both the inner and outer orbits. The precession period is about 25 yr. (The theoretical value is $P_{\rm node} = 25.0 \pm 0.1$ yr.) In these panels, we also denote with cyan (or green) regions of the inclination-angle domain where both (or at least one) eclipses of the inner binary can be observed. The borders of these regions are calculated from the equation

$$|\cos i_{\rm in}| = \frac{R_{\rm Aa} + R_{\rm Ab}}{a_{\rm in}} \frac{1 \pm |e_{\rm in} \sin \omega_{\rm in}|}{1 - e_{\rm in}^2}, \quad (2)$$

whereas, on the right-hand side, the positive sign gives the inclination-angle limit for a single eclipse (i.e. the green area), while the negative sign gives the limit where both eclipses should occur (the cyan area). As one can see, during the first part of the *Kepler*-observations, the inner inclination became closer and closer to 90°, and the inner orbit was seen exactly edge-on from the Earth around 2011.5. Therefore, during the second part of the *Kepler* measurements, the orbital plane was viewed under a continuously decreasing angle. This is in nice agreement with the first increasing, then constant (total eclipses) and, finally, decreasing eclipse depths (Fig. 1) that were seen. Moreover, one can also see in the lower left-hand panel of Fig. 7 that during sectors 14 and 15 *TESS*-observations (≈2019.6), the inner binary was at the very edge of the eclipsing regime. Strictly speaking, the inner eclipses were present, however, their amplitudes were two orders of magnitude smaller than the scatter of the *TESS* light curve of this very faint ($T = 15.0$ mag) source. And, indeed, no third-body eclipse was seen during the two sectors of *TESS* observations, therefore, the eclipsing nature of this system remained hidden from *TESS*. In contrast to this, during the scheduled sectors 54 and 55 observations (≈2022.6) the inner binary will again be very close to its next edge-on position ($i_{\rm in} \approx 90\overset{\circ}{.}7$), offering much better conditions to observe the shallow regular eclipses.

In the same panels we also denote, with thin black lines, the inclination limits of the outer inclination domain for the possibility of third-body eclipses. These are defined as follows:

$$|\cos i_{\rm out}| = \frac{R_{\rm B} + R_{\rm Ab} + \frac{a_{\rm in}}{1+q_{\rm out}} \left(1 + \tan^2 i_{\rm in} \cos^2 \Delta\Omega\right)^{-1/2}}{a_{\rm out}} \times \frac{1 + |e_{\rm out} \sin \omega_{\rm out}|}{1 - e_{\rm out}^2}. \quad (3)$$

(We will discuss this expression in Appendix A.) As one can see, the system continuously remains in the domain of the third-body eclipses.

In addition, we assess the long-term future evolution of KIC 6964043. On longer time-scales of a few 100 Myr (Fig. 8), KIC 6964043 displays evolution of the eccentricity of the outer orbit due to the octupole term. The outer eccentricity slowly increases from the initial value of ≈0.48 to ≈0.50 at 765 Myr. At this point, the system formally crosses into the dynamically unstable regime. Given the current proximity to the stability limit, it is not surprising that the system's hierarchy may break down. As the secular theory that *TRES* is based on is no longer valid at this point, we stop the simulation. Based on Toonen et al. (2022), we expect the system to remain in the dynamically unstable regime as an unstable but bound triple for on average $10^4$ crossing times, about 5 kyr. The most likely outcome of such an interaction is the dissolution of the system into a binary and single star, or the collision of two of the stars reducing the system

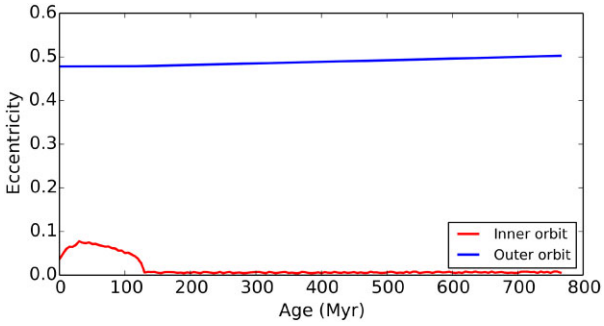


**Figure 8.** Evolution of the system eccentricities in KIC 6964043.

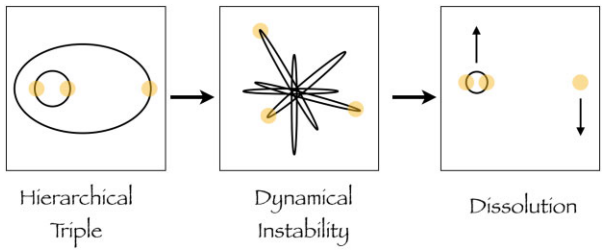


**Figure 9.** Schematic evolution of the triple star system KIC 6964043.

from a triple into a binary. A summary of the evolution in shown in Fig. 9.

### 5.2 KIC 5653126

This triple contains the most massive stars in our sample, and it has the second highest inner and outer mass ratios ($q_{\rm in} = 0.736 \pm 0.006$; $q_{\rm out} = 0.418 \pm 0.004$). The most massive component is the early F-type primary of the inner pair ($m_{\rm Aa} = 1.77 \pm 0.03\,{\rm M}_\odot$; $R_{\rm Aa} = 2.20 \pm 0.02\,{\rm R}_\odot$; $T_{\rm eff,Aa} = 7060 \pm 80$ K), while its binary companion and the tertiary star are very similar late F-type stars ($m_{\rm Ab} = 1.30 \pm 0.02\,{\rm M}_\odot$; $R_{\rm Ab} = 1.31 \pm 0.02\,{\rm R}_\odot$; $T_{\rm eff,Ab} = 6260 \pm 60$ K and $m_{\rm B} = 1.29 \pm 0.03\,{\rm M}_\odot$; $R_{\rm B} = 1.28 \pm 0.04\,{\rm R}_\odot$; $T_{\rm eff,B} = 6230 \pm 60$ K). The age of the system is found to be $\tau = 1.0 \pm 0.1$ Gyr. Our analysis yields a distance of $d = 1375 \pm 15$ pc, which agrees with the trigonometric Gaia EDR3 distance to within $3\sigma$.

Turning to the orbital parameters, both the inner and outer orbits are moderately eccentric ($e_{\rm in} = 0.294 \pm 0.002$ and $e_{\rm out} = 0.179 \pm 0.001$). The mutual inclination of the orbital planes was found to be $i_{\rm mut} = 12\overset{\circ}{.}3 \pm 0\overset{\circ}{.}2$, but at that epoch both orbits had very similar observable inclination angles. At the beginning of the *Kepler* observations, the inclination angles were $i_{\rm in} = 87\overset{\circ}{.}13 \pm 0\overset{\circ}{.}02$ and $i_{\rm out} = 87\overset{\circ}{.}6 \pm 0\overset{\circ}{.}5$ for the inner and outer orbital planes, respectively. Note that, despite the absence of third-body eclipses, which would strongly constrain the outer inclination angle as well as the mutual inclination, we were able to find these quantities with remarkable accuracies of some tenths of a degree (which is even better than the accuracies obtained for the same parameters in the case of some *TESS* observed triply eclipsing triples – see e.g. Borkovits et al. 2022). This is a consequence of the fact that the variation of the inner inclination angle and, hence, the depths and durations of the inner eclipses are extremely sensitive to these parameters. (Note, for the former system, KIC 6964043, where both the EDVs and third-body eclipses were detected continuously over a 3-yr-long time-scale, we were able to obtain even higher accuracies, some hundredths of a degree, for these parameters.)

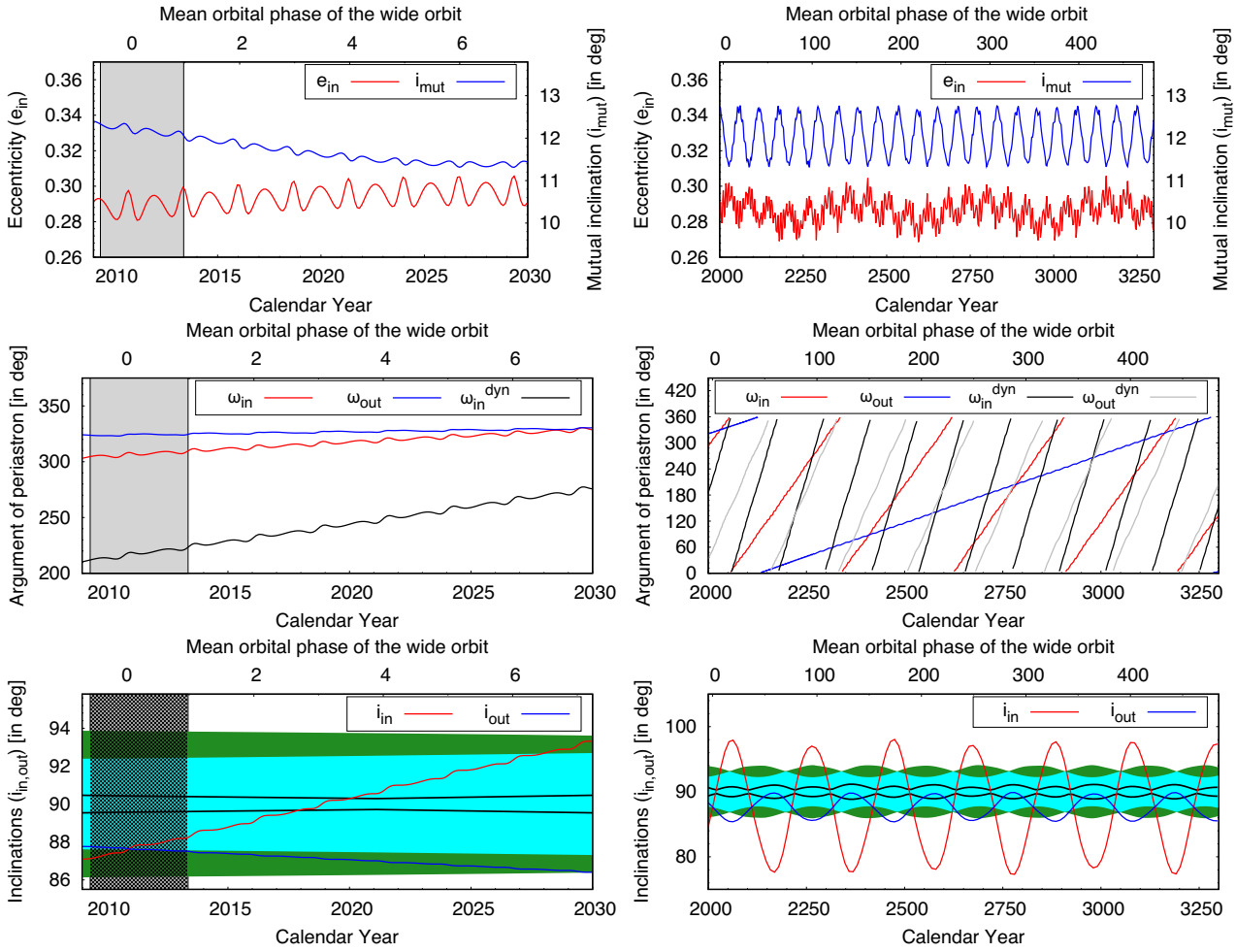


**Figure 10.** Variations of the same orbital elements as in Fig. 7 above, but for KIC 5653126. Note, that the right-hand panels here and also in the similar plots of the other two systems below, represent an interval of 1300 yr in contrast to the 250 yr shown in the right panels of Fig. 7 for KIC 6964043. See text for details.

At this point, we comment on the presence or absence of third-body eclipses. In contrast to the triply eclipsing triple KIC 69640433, in the case of this, and the other two systems, we will discuss, in the absence of third-body eclipses, the light curves do not carry any information on the radii and effective temperatures of the tertiary components, because their only direct effects on the light curves are the dilution of the regular eclipses by their extra flux contamination. Thus, the third star's radius and temperature are largely dependent on the PARSEC isochrones. The latter, however, are constrained by the third star's mass and mass ratios, which can be inferred quite accurately from the photodynamical analysis. This is especially true of the effects of the third-body perturbations that drive apsidal motion, leading to ETVs, and orbital plane precession (whose consequences were discussed in the preceding paragraph). Thus, the fact that the dynamically inferred third star masses led to fully consistent MDN solutions, in our view, again verifies the use of PARSEC isochrones as proxies either for the masses (in the absence of RV data in the case of regular EBs) or radii and other fundamental stellar parameters (in the absence of third-body eclipses).

Turning now to the above-mentioned perturbations, in Fig. 10 we display the variations of some orbital elements over 30 and ≈1300 yr-long intervals. In contrast to KIC 6964043, besides the characteristic medium ($P_{\rm out}$) time-scale perturbations (upper left-hand panel), now some longer time-scale periodic variations can be identified both in the inner eccentricity and the mutual inclination. The amplitudes of these clearly exceed those of the medium period effects, though the relative variations in both orbital elements remain at the few per cents level. As one can see, $e_{\rm in}$ and $i_{\rm mut}$ vary in an anticorrelated manner, and the characteristic period of these cycles is about half of the dynamical apsidal motion period. These findings are in good agreement with the theories of the quadrupole-order long-period perturbations in the low mutual inclination regime (see e.g. Mazeh & Shaham 1979; Söderhjelm 1982; Borkovits et al. 2007). Moreover, another even longer period variation in the eccentricity can also be noticed, which we attribute to the octupole-order perturbations (e.g. Naoz et al. 2013). These variations, however, again remain small, and our longer, 1 million yr numerical integration displays the same picture.

The variations of the observationally more relevant orbital elements, again, are shown in the middle (apsidal motion) and bottom (orbital precession) panels. The behaviour of the different arguments of periastron are similar to those of KIC 6964043, but the periods are somewhat longer, in accordance with the longer characteristic time-scale of $P_{\rm out}^2/P_{\rm in}$. The calculated (theoretical) observable apsidal motion periods are $P_{\rm apse,\,in} = 309 \pm 4$ yr and $P_{\rm apse,\,out} = 1204 \pm 4$ yr for the inner and outer orbits, respectively. Besides the longer time-scales, another minor difference in the behaviour of the rotations of the lines of the apsides relative to the previous system is that the dynamical apsidal motion no longer remains strictly linear, but

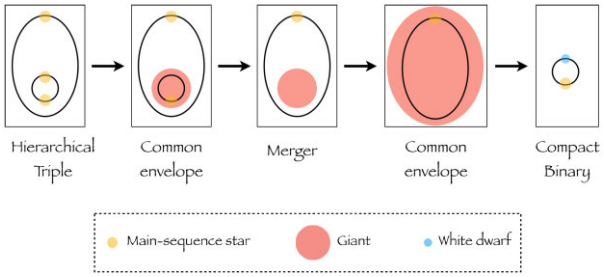


**Figure 11.** Schematic evolution of the triple star system KIC 5653126.

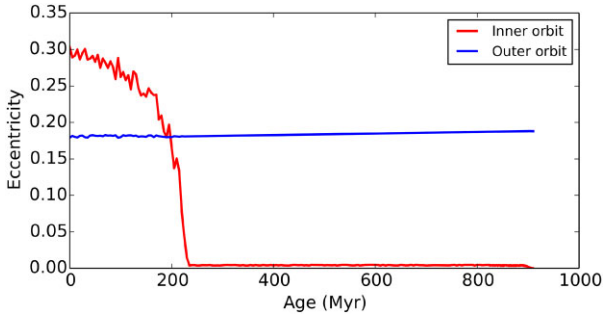


**Figure 12.** Evolution of the system eccentricities in KIC 5653126.

a low-amplitude cyclic variation (with a period similar to that of the eccentricity variation period) is also superposed on the linear trend. For such a low mutual inclination, however, the amplitude of this extra cyclic term, from an observational point of view, remains negligible.

In the bottom panels, the variations of the observable inclination angles, and the domains within which eclipses are possible are plotted. The precession period is calculated to be $P_{\rm node} = 225 \pm 3$ yr. During one cycle, the inner binary exhibits eclipses only in two, separated, ≈40 yr-long intervals. The current eclipsing session will terminate at the very end of 2031. What is more interesting is that there are short intervals when third-body eclipses are also possible. The last such interval of outer eclipses occurred circa the 1970s. In order to check whether third-body eclipses had actually occurred during that period, we back-integrated our best solution (i.e. the set of input parameters which yielded the lowest net $\chi^2$ value) to 1950, and found two third-body events during 1976 January 12–14 and 1978 September 11–15. The same integration has revealed that the next third-body eclipse is expected only in the year 2143. As one can see in the lower-right panel of Fig. 10, these third-body eclipses may occur when the inner binary is the farthest from its EB state. At the current time, only one such triple star system is known with certainly, and it currently shows third-body eclipses without inner binary eclipses. This is KIC 2835289, a 0.86-d-period ellipsoidal variable, orbited by a third star with a period of $P_{\rm out} = 755$ d, from which two third-body eclipses were observed with *Kepler* (Conroy et al. 2014; Conroy K., Prša & Stassun 2015), and a further one with *TESS*. Moreover, Borkovits et al. (2020a) found that TIC 167692429, which currently is an EB with remarkable EDVs, has also produced third-body eclipses in the recent past, *before* the beginning of its recent eclipsing session. And, the last of those events was actually identified with great likelihood in the archival SuperWASP observations of that triple.

As with KIC 6964043, we address the long-term future evolution of KIC 5653126 by making use of the *TRES* code. The long-term future of KIC 5653126 is different that of the previous system as in the case of KIC 5653126 the stars are massive enough to evolve off the MS in a Hubble time (see Fig. 11). As the primary of the inner binary, which is the most massive star in this triple ascends the first giant branch and expands rapidly, the system changes due to three reasons; (1) tidal torques amplify leading to the near circularization of the inner binary (Fig. 12). The inclination freezes out at about 30 degrees, after increasing steadily from the current inclination of about 12 degrees. (2) the primary star loses 0.004 $M_\odot$ of envelope material due to its stellar winds. As a result, there is a slight increase in the outer semimajor axis from 675.8 to 676.42 $R_\odot$. There is also a widening effect from the wind mass loss on the inner orbit, however, the dominant effect is a slight shrinkage of the semimajor axis from 69.77 to 69.46 $R_\odot$ due to stellar tides. (3) Lastly, and most importantly, at 1910 Myr, the primary star fills its Roche lobe.

Given the evolutionary state of the donor star and its deep convective envelope, the ensuing mass transfer phase proceeds in an unstable way, quickly leading to a CE phase (for a review, see Ivanova et al. 2013). During this phase, the secondary star orbits around the core of the primary star inside its envelope. Friction causes the secondary's orbit to decay leading to the merger of the secondary with the core of the star, or a tight binary if the envelope can be ejected. Adopting the classical energy-based CE-prescription (i.e. the $\alpha$-model; Paczynski 1976; Webbink 1984; Livio & Soker 1988; de Kool 1990), the CE-phase leads to a merger of the two stars in the inner binary. This holds for both the classical values of the CE-efficiency ($\alpha \approx 1$), as well as the observationally derived reduced efficiencies ($\alpha \approx 0.25$; Zorotovic et al. 2010; Toonen & Nelemans 2013; Camacho et al. 2014; Zorotovic et al. 2022). The resulting merger product is a giant-like object with a compact helium-rich core of 0.32 $M_\odot$ and a massive hydrogen-rich envelope of 2.75 $M_\odot$, assuming a conservative merger.

As this object evolves further, it will initiate core helium burning followed by helium-shell burning as it ascends the asymptotic giant branch (AGB). During this phase, when the merger remnant is still orbited by the initial tertiary star, it fills its Roche lobe again. This second CE-phase does not lead to a merger, as the pre-CE orbit is much wider than for the first CE-phase. After the second CE-phase, the system consists of a 0.65 $M_\odot$ white dwarf (i.e. the old core of the AGB-star) and a 1.29 $M_\odot$ main-sequence companion. The orbit of the post-CE system depends critically on the CE-efficiency i.e. the efficiency with which the orbital energy is converted to unbind the envelope. In both cases of inefficient ($\alpha = 1$) and efficient ($\alpha = 0.25$) CE-evolution, the system experience an ultimate mass transfer event, with the white dwarf as the accretor star, and the donor star either on the main-sequence or giant branch, respectively. In both cases, the system ends its life as a single white dwarf of mass 0.8–0.9 $M_\odot$. Even though the systems started out its life as a triple star system, we expect it will end its life as a single star.

### 5.3 KIC 5731312

Now we turn to the two dynamically more interesting, high mutual inclination systems. KIC 5731312 is the least massive triple in our sample. The inner binary is formed by a K and an M-type dwarf ($m_{\rm Aa} = 0.77 \pm 0.01\,M_\odot$; $R_{\rm Aa} = 0.73 \pm 0.01\,R_\odot$; $T_{\rm eff,Aa} = 5080 \pm 60$ K and $m_{\rm Ab} = 0.51 \pm 0.02\,M_\odot$; $R_{\rm Ab} = 0.51 \pm 0.03\,R_\odot$; $T_{\rm eff,Ab} = 3690 \pm 30$ K, respectively), while the distant, third component is a very low-mass, cool, late M star ($m_{\rm B} = 0.15 \pm 0.01\,M_\odot$; $R_{\rm B} = 0.18 \pm 0.01\,R_\odot$; $T_{\rm eff,B} = 2910 \pm 30$ K). Thus, the mass ratios are far from unity ($q_{\rm in} = 0.665 \pm 0.040$; $q_{\rm out} = 0.120 \pm 0.004$) and, in such

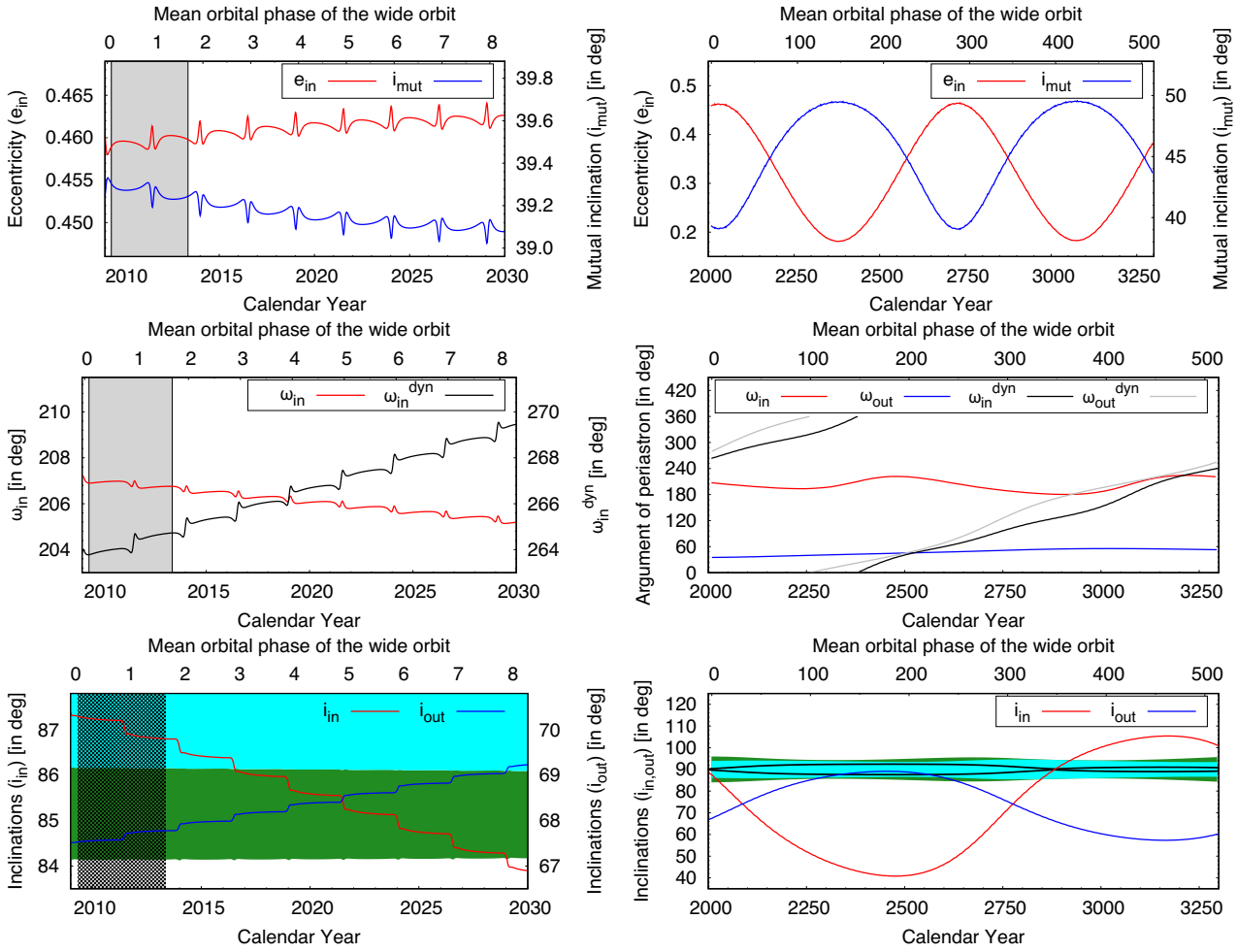


**Figure 13.** Variations of the same orbital elements as in Fig. 7 above, but for KIC 5731312. See text for details.

a way, they differ substantially from the mass ratios of the flat triples investigated above. This fact, together with the inclined tertiary orbit, certainly imply a different formation scenario. The system is found to be quite old ($\tau = 5.9 \pm 0.6$ Gyr). Its photodynamically obtained distance ($d = 353 \pm 7$ pc) is in excellent agreement with the Gaia EDR3 distance.

As mentioned in Section 2, this triple is by far the least tight one in our sample ($P_{\rm out}/P_{\rm in} \approx 122$). Moreover, the outer mass ratio is also very low. As a consequence, one can observe remarkable, readily detectable ETVs in this system largely due to the high inner and outer eccentricities ($e_{\rm in} = 0.4587 \pm 0.0005$ and $e_{\rm out} = 0.575 \pm 0.008$). In an opposite, i.e. nearly circular, case, the presence of the distant tertiary probably would have remained unnoticed even via an ETV analysis based on the highly accurate timing data that were obtained from *Kepler* observations. While the semimajor axes of the two orbits are found to be $a_{\rm in} = 18.2 \pm 0.1\,{\rm R}_\odot$ and $a_{\rm out} = 448 \pm 2\,{\rm R}_\odot$, respectively, at the times of apastron passage of the inner orbit, and periastron passage of the outer orbit, the orbital separations are $r_{\rm in}^{\rm apo} \approx 26.5\,{\rm R}_\odot$ and $r_{\rm out}^{\rm peri} \approx 190.6\,{\rm R}_\odot$. Hence, the ratio of the equivalent periods becomes $P_{\rm out}^{\rm peri}/P_{\rm in}^{\rm out} \approx 19.2$, temporarily resulting in a very tight triple system.

The mutual inclination of the two orbits is found to be $i_{\rm mut} = 39\overset{\circ}{.}4 \pm 0\overset{\circ}{.}3$, i.e. the former findings of Borkovits et al. (2015, 2016), which were based only on an analytic analysis of the ETV curves, is nicely confirmed. This mutual inclination value is very close to the famous mutual inclination limit ($i_{\rm mut}^{\rm ZKL} = 39\overset{\circ}{.}23$, and its retrograde counterpart) of the original, quadrupole, asymptotic ZKL theory, which separates the low- and high mutual inclination regimes of the phase space (see the short summary in the Introduction). However, as discussed next, the configuration of the present system is far from appropriate to be fit in the framework of the original ZKL theory. Due to the large outer eccentricity and small inner mass ratio, the octupole-order perturbations may become significant, and hence the evolution of the orbital elements should be modelled within the framework of the eccentric ZKL formalism (see e.g. Naoz 2016).

First we introduce again the short-term characteristics of these perturbations in some of the orbital elements, as well as their direct observational consequences. In order to do this, similar to the previous two triples, we display decades and centuries long variations of a few orbital elements obtained from a 1-Myr-long numerical integration in the various panels of Fig. 13. Now the eccentricity cycles of the inner binary, and the corresponding variations of the mutual inclination with a period of $P_{\rm ZKL} \approx 690$ yr and full amplitudes of $\Delta e_{\rm in} \approx 0.28$ and $\Delta i_{\rm mut} \approx 10^\circ$ are clearly visible in the upper panels. The characteristics of these variations do not change significantly during the entire 1-million-yr integration, however, a slow sinusoidal variation in the amplitudes of $\approx 10$ per cent on an $\approx 10000$ yr timescale is also apparent, probably due to the octupole terms.

As one can see in the middle-left panel, the inner EB exhibits retrograde apsidal motion in the observational frame over the current

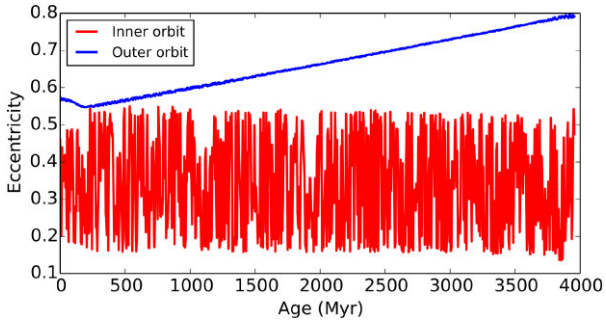


**Figure 14.** Evolution of the system eccentricities in KIC 5731312.

several decades. This results because a negative contribution arises from the nodal regression, which temporarily overpowers the effect of the prograde apsidal advance in the dynamical frame of reference. However, as the middle-right panel shows, this is only part of a longer-term oscillatory (i.e. libration) cycle. The dynamical apsidal motion of both the inner and outer orbits remain continuously prograde, however, their non-linear nature, i.e. the presence of a significant librating motion in addition to the usual circular apsidal motion is readily visible in the middle-right panel. Their period is about 1300–1400 yr, i.e. twice of that of the eccentricity cycles (which, again, is in perfect agreement with the theory of the secular perturbations). Note, however, that these values do not agree with the theoretical apsidal motion periods tabulated in Table 3. The reason is that these latter periods were calculated from the instantaneous apsidal motion rates (also listed in the tables) simply by linear interpolation and, hence, do not give accurate results for highly non-linear apsidal motions.

The variations in the visible inclination angles are shown in the bottom panels of Fig. 13. The nodal precession cycle of this triple has a period of $P_{\rm node} \approx 1400$ yr. During such a cycle, the inner pair of stars exhibits eclipses only for two short, 80–100 yr-long intervals. The current eclipsing session began around the 1950s, and the EB was seen edge-on at the beginning of the 1990s. During the prime *Kepler* mission, both kinds of eclipses were observable. Then, however, the eclipse closer to apastron would no longer have been observable since ∼2016.5, which is in accord with the 2019 and 2021 *TESS* measurements. The remaining solo eclipses will also disappear in about 2029.0, and the eclipses will return only in the XXIX-th century. Finally, as one can see, between circa 2300 and 2600, there might be a chance for third-body eclipses to appear. In order to check this possibility, we numerically generated the system's light curve for a section of this interval, and found two very shallow (with depth of ∼ 0.3 per cent) third-body eclipses at the epoch 2453.63.

The long-term future of KIC 5731312 is reminiscent of that of KIC 6964043 (see Fig. 9). On long time-scales, here of the order of more than a few Gyr, we find an extra modulation in the eccentricity of the outer orbit due to the octupole term (Fig. 14). The eccentricity first decreases from the original value of ≈0.57–0.55, after which it starts increasing. When the outer eccentricity reaches a value of ≈0.81 at 3.96 Gyr, the system crosses the stability limit, in analogy of KIC 6964043. Given the stellar masses of KIC 5731312, the stars are still on the MS when this happens, and will remain so within a Hubble time. The evolution during the dynamically unstable phase is therefore a pure dynamical (gravitational) problem. After many crossing times ($10^4$ crossing time is about 0.75 kyr), the system most likely dissolves into a bound binary and a single star ejecting the low-mass tertiary star from the system.

### 5.4 KIC 8023317

This triple has the most extreme inner and outer mass ratios in our sample ($q_{\rm in} = 0.303 \pm 0.013$; $q_{\rm out} = 0.079 \pm 0.003$). The main stellar component is one of the EB stars, and is a slightly evolved G-type star ($m_{\rm Aa} = 1.30 \pm 0.07\,{\rm M}_\odot$; $R_{\rm Aa} = 1.96 \pm 0.05\,{\rm R}_\odot$; $T_{\rm eff,Aa} = 5870 \pm 70$ K). Its binary companion is a low-mass M-type red dwarf ($m_{\rm Ab} = 0.39 \pm 0.01\,{\rm M}_\odot$; $R_{\rm Ab} = 0.39 \pm 0.01\,{\rm R}_\odot$; $T_{\rm eff,Ab} = 3165 \pm 45$ K). The tertiary is another even lower-mass M star with $m_{\rm B} = 0.13 \pm 0.01\,{\rm M}_\odot$, $R_{\rm B} = 0.17 \pm 0.01\,{\rm R}_\odot$, and $T_{\rm eff,B} = 2575 \pm 35$ K. The latter star has the lowest mass among all dozen in our full sample. The age of the triple is found to be $\tau = 4.3 \pm 0.5$ Gyr. The photodynamically obtained distance is $d = 814 \pm 20$ pc, which is larger than the Gaia EDR3 inferred distance by about $3\sigma$.

The mutual inclination is found to be $i_{\rm mut} = 55\overset{\circ}{.}7 \pm 0\overset{\circ}{.}8$, which is even higher by ∼6° than the former result of Borkovits et al. (2015, 2016). Thus, according to our knowledge, this system has the second-highest mutual inclination after Algol amongst all triple star systems with accurately known mutual inclinations.

The ZKL cycles in the inner eccentricity and the mutual inclination are, again, clearly visible (see upper panels of Fig. 15) and look quite similar to those same features of the previous system, KIC 5731312. One quantitative difference, however, is that the ZKL cycle period is shorter, being $P_{\rm ZKL} \approx 360$ yr, in accordance with the shorter $P_{\rm out}^2/P_{\rm in}$ time-scale. The ranges of the variations of both parameters are very close to that of KIC 5731312, but the phase is almost opposite. While KIC 5731312 currently is close to its maximum eccentricity and, hence, minimum mutual inclination phase, KIC 8023317, is close to its smallest inner eccentricity, and largest mutual inclination.

There is, however, an important qualitative difference in the behaviour of the apsidal lines of the inner orbits between the present and the previous system. While in the case of KIC 5731312, the dynamical apsidal line circulates, in the case of KIC 8023317, it librates around $\omega_{\rm in}^{\rm dyn} = 90°$, with a half-amplitude of ≈27°. The period of this libration is the same as that of the inner eccentricity cycles. Though prior numerical (e.g. Ford et al. 2000) and theoretical works (Naoz 2016) have shown that the periods of apsidal librations and circulations may alter each other, in the present situation, the libration remained unchanged throughout our 1-Myr-long numerical integration. Regarding the observable apsidal motion of the inner pair, it is again clearly retrograde, as can be seen nicely in the middle panels of Fig. 15.

Finally, we consider the variations of the inclination angles in the bottom panels of Fig. 15. The precession period is about $P_{\rm node} \approx 650$ yr. The current eclipsing session of the inner pair started around 2000.0, and central eclipses will occur around 2023.7. The eclipses will then completely disappear around 2052.7, and will return only near the beginning of 2088. Moreover, similar to the other three triples studied in this work, third-body eclipses are also possible during given sections of a precession cycle. In contrast to the previous systems, however, in the case of KIC 8023317, the outer inclination crosses both the lower and upper borders of the possible third-body eclipse regions (and hence, the outer orbit may also be seen edge-on two times during a precession cycle). The next session of possible third-body eclipses will begin around 2354 and last until 2404.

The long-term evolution of KIC 8023317 is similar to that of KIC 5653126 (see Fig. 11). The primary star is massive enough to evolve off the main-sequence at 4.7 Gyr and fill its Roche lobe as it ascends the first giant branch at 5.3 Gyr. At this point the primary star has lost a small amount of mass due to its stellar wind, i.e. 0.004 $M_\odot$, such that the outer semimajor axis has increased by 0.2 per cent. The inner orbit did not widen, in fact the inner semimajor axis was

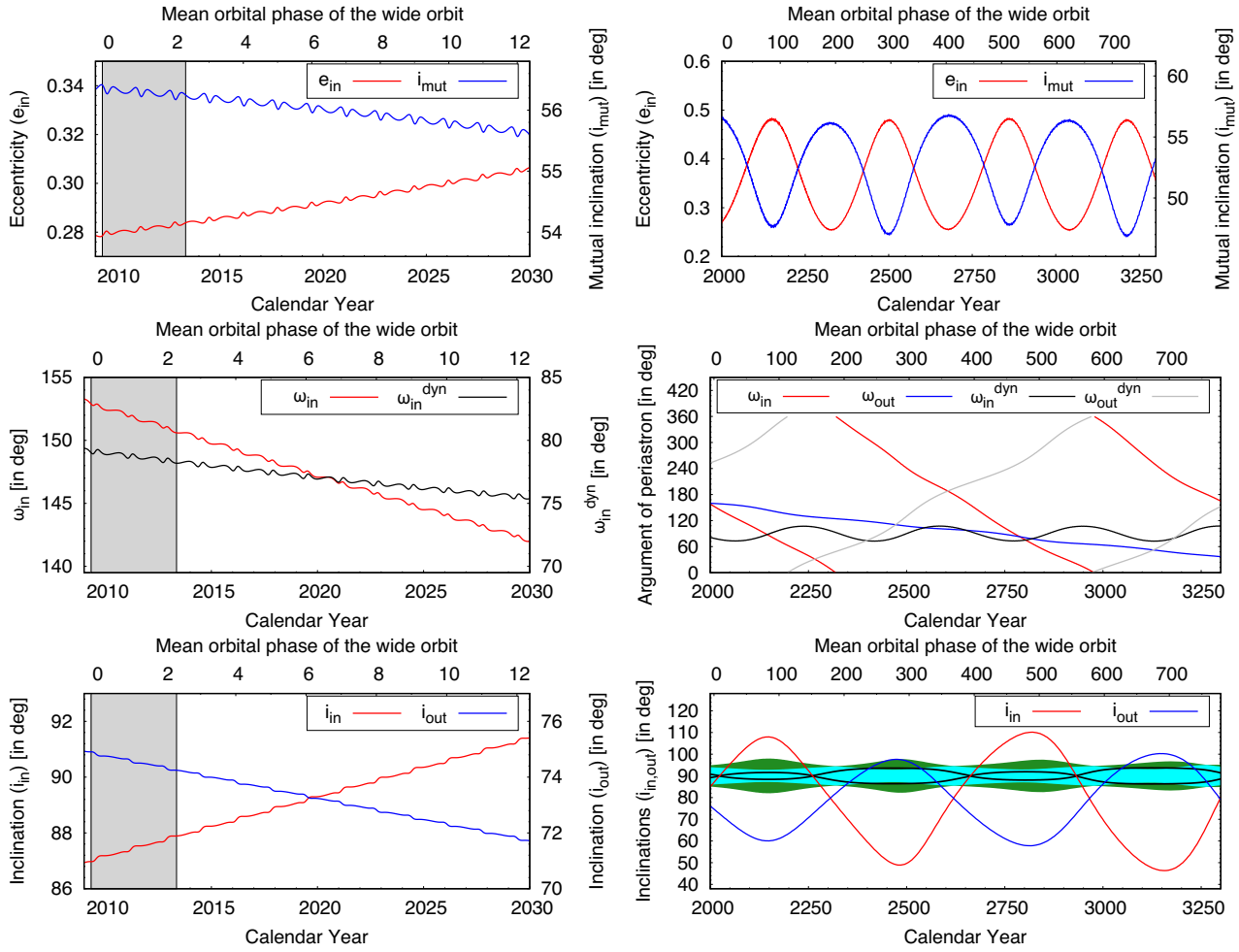


**Figure 15.** Variations of the same orbital elements as in Fig. 7 above, but for KIC 8023317. See text for details.

reduced from the original 32.6 to 24.5 $R_\odot$ due to tidal friction in combination with ZKL cycles (Kiseleva, Eggleton & Mikkola 1998). Furthermore, the inner orbit has circularized by the time of the onset of the mass transfer phase and the inclination freezes out at about 41 degrees. With the extreme mass ratio of the inner binary, the mass transfer leads to a CE phase and a subsequent merger of the two stars in the inner binary. The merger remnant is a giant-like object with a helium core of 0.24 $M_\odot$ and a relatively thick envelope of at most 1.44 $M_\odot$. In analogue with KIC 5653126, the merger remnant will fill its Roche lobe as an AGB star, initiating a second CE-phase. A compact binary is formed with a 0.52 $M_\odot$ white dwarf component and a 0.13 $M_\odot$ main-sequence companion. In the case of an efficient CE-phase, the post-CE semimajor axis is about 8 $R_\odot$. In the inefficient case it is ∼1 $R_\odot$, which is compact enough such that magnetic braking and gravitational wave emission can reduce the orbit to form a cataclysmic variable in a Hubble time.

### 5.5 Implications of the results for different multiple star formation processes

As indicated above, there appears to be an anticorrelation between the mutual inclination and tertiary mass. Our two highly misaligned triples, KIC 5731312 with $i_{\rm mut} = 39^\circ$ and KIC 8023317 with $i_{\rm mut} = 56^\circ$, both contain low-mass M5/6V tertiaries with $m_{\rm B} = 0.13 - 0.15\,M_\odot$. Meanwhile, our two relatively aligned triples have more comparable component masses. To determine if this trend is statistically significant, we expand our sample to include all of our previously analysed triples with reliably measured mutual inclinations and outer mass ratios $q_{\rm out} = m_{\rm B}/(m_{\rm Aa} + m_{\rm Ab})$. From the Borkovits et al. (2016) sample of 62 compact *Kepler* triples with measured mutual inclinations, we update the four systems presented in this study with the current, more accurate photodynamical results. We also update KIC 7955301 with $i_{\rm mut} = 6.2^\circ$ and $q_{\rm out} = 0.71$ according to our upcoming photodynamical analysis (Gaulme et al., in preparation). We exclude KIC 3345675 and KIC 7593110, which have large mutual inclination uncertainties that exceed $\delta i_{\rm mut} > 10^\circ$. We also ignore the only retrograde triple, KIC 7670617 with $i_{\rm mut} = 147^\circ$, which likely formed differently than the remaining 59 KIC prograde triples spanning $0^\circ < i_{\rm mut} < 56^\circ$. We also add the 12 recently discovered *TESS* triples, most of which are nearly coplanar triply eclipsing systems (Mitnyan et al. 2020; Borkovits et al. 2020a, b, 2022; Rappaport et al. 2022). None the less, TIC 042565581 is slightly misaligned with $i_{\rm mut} = 5.5^\circ$ and $q_{\rm out} = 0.65$ while TIC 167692429, (the only one currently non-eclipsing *TESS* triple) is moderately misaligned with $i_{\rm mut} = 27^\circ$ and $q_{\rm out} = 0.34$.

A Spearman rank correlation test demonstrates that the mutual inclinations and outer mass ratios of our selected 71 compact triples are anticorrelated with a coefficient of $\rho_{\rm S} = -0.40$ and statistical significance of $p_{\rm S} = 0.0006$ ($3.5\sigma$). In Fig. 16, we plot the distributions of $q_{\rm out}$ for three subsamples: (1) the 29 nearly coplanar

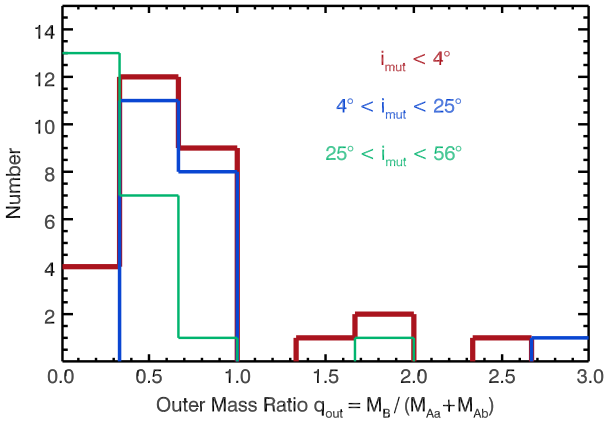


**Figure 16.** The distributions of outer mass ratios for the 29 nearly coplanar triply eclipsing systems with $i_{\rm mut} < 4^\circ$ (thick red), the 20 moderately misaligned triples with $4^\circ \leq i_{\rm mut} < 25^\circ$ (blue), and the 22 highly misaligned triples with $25^\circ \leq i_{\rm mut} < 56^\circ$ (thin green). More coplanar triples tend to have more massive outer tertiaries, suggesting that compact triples accreted from surrounding protostellar discs that simultaneously aligned the orbits while leading to preferential mass accretion on to the outer tertiaries.

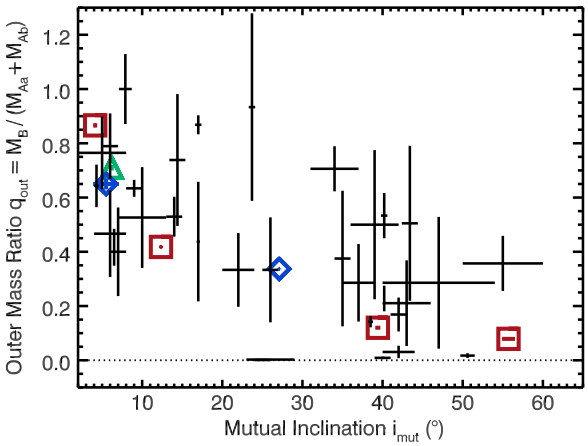


**Figure 17.** Outer mass ratios versus mutual inclinations for the 40 compact triples with $4^\circ \leq i_{\rm mut} < 56^\circ$ and $q_{\rm out} \leq 1.0$. We highlight the 4 KIC triples presented in this study (red boxes), the two misaligned TIC triples (blue diamonds), and the Gaulme et al. preliminary result for KIC 7955301 (green triangle). The outer mass ratios systematically decrease with mutual inclination at the $4.5\sigma$ level. A more massive tertiary likely accreted from a massive circumtriple protostellar disc that aligned both the inner and outer orbits with the disc.

triply eclipsing systems with $i_{\rm mut} < 4^\circ$ that are subject to different selection effects than the non-triply eclipsing systems; (2) the 20 somewhat misaligned triples with $4^\circ \leq i_{\rm mut} < 25^\circ$; and (3) the 22 highly misaligned triples with $25^\circ \leq i_{\rm mut} < 56^\circ$. The nearly coplanar triples are concentrated across $q_{\rm out} = 0.33$ - 1.00, but there are a few systems below $q_{\rm out} < 0.33$ and above $q_{\rm out} > 1.00$. Similarly, all but one of the 20 somewhat misaligned triples span $q_{\rm out} = 0.33$–1.00. The single outlier with $q_{\rm out} = 3.0$ and $i_{\rm mut} = 8^\circ$ is KIC 5897826, which is barely a triply eclipsing system (Carter et al. 2011). Meanwhile, more than half of the highly misaligned triples have small-mass ratios $q_{\rm out} < 0.33$. The single outlier with $i_{\rm mut} = 54^\circ$ and $q_{\rm out} = 1.8$ is KIC 4055092, which has one of the widest tertiaries with $a_{\rm out} = 11$ au and therefore likely formed differently from the more compact triples in our sample.[13] The Anderson–Darling test demonstrates that the somewhat misaligned and highly misaligned triples have different $q_{\rm out}$ distributions at the $p_{\rm AD} = 8 \times 10^{-6}$ ($4.3\sigma$) significance level. Moreover, if we limit our sample to the 40 triples with $4^\circ \leq i_{\rm mut} < 56^\circ$ and $q_{\rm out} \leq 1.0$, then a Spearman rank test yields an even stronger degree of anticorrelation with $\rho_{\rm S} = -0.66$ and $p_{\rm S} = 4 \times 10^{-6}$ ($4.5\sigma$). The anticorrelation between the mutual inclinations and outer mass ratios for this subset of 40 compact triples is clearly visible in Fig. 17.

Compact triples with $a_{\rm out} \lesssim 10$ au likely formed either through two successive episodes of disc fragmentation or disc-mediated capture of the outer tertiary (Tobin et al. 2016; Bate 2018; Tokovinin & Moe 2020; Offner et al. 2022). In both scenarios, the tertiary tends to be initially less-massive than the inner binary, but the triple subsequently accretes from the surrounding protostellar disc. For an isolated protobinary that accretes from a circumbinary disc, the low-mass secondary sweeps out a larger orbit and thus accretes most of the infalling material, effectively driving the binary mass ratio $q = M_2/M_1$ towards larger values (Bate & Bonnell 1997; Farris et al. 2014; Young & Clarke 2015). Close binaries exhibit a large excess of twins with $q > 0.95$ (Tokovinin 2000; Moe & Di Stefano 2017; El-Badry et al. 2019; Tokovinin & Moe 2020), consistent with the predictions of the hydrodynamical simulations of circumbinary disc accretion. Similarly, a low-mass tertiary in a compact triple will accrete most of the mass from the circumtriple disc, thereby increasing the outer mass ratio $q_{\rm out}$ (Tokovinin & Moe 2020).

For a protobinary with small-to-moderate eccentricity, circumbinary disc accretion also tends to align the binary orbit to the plane of the disc (Papaloizou & Terquem 1995; Lubow & Ogilvie 2000; Lodato & Facchini 2013; Foucart & Lai 2014; Martin, Zhu & Armitage 2020). Close pre-MS binaries undergo tidal circularization (Meibom & Mathieu 2005; Moe & Kratter 2018; Zanazzi & Wu 2021). Indeed, pre-MS binaries with $P < 30$ d have small-to-moderate eccentricities and nearly coplanar circumbinary discs as expected Czekala et al. (2019). A significant majority of the inner binaries in our sample of compact triples also have small-to-moderate eccentricities and short periods, and so we expect the inner binary and circumbinary disc to have aligned prior to the formation or disc-capture of the tertiary. A notable exception includes KIC 5731312 investigated in this study, which has an inner binary with a relatively large eccentricity $e_{\rm in} = 0.46$ given its short period of $P_{\rm in} = 7.95$ d. None the less, KIC 5731312 also has a highly inclined tertiary with $i_{\rm mut} = 39.4^\circ$, precisely matching the critical von Zeipel-Kozai-Lidov angle (see Section 5.3), and suggesting this particular triple dynamically evolved via ZKL cycles coupled to tidal friction (Kiseleva et al. 1998; Fabrycky & Tremaine 2007; Naoz & Fabrycky 2014). For the rest of our systems, once the tertiary forms in the outer disc via disc fragmentation (born nearly coplanar) or is captured by the disc, subsequent inclination evolution of the tertiary depends on the mass of the disc (Martin et al. 2016). For massive discs, the tertiary accretes much of the mass and angular momentum from the disc, thereby dissipating into a coplanar configuration. Meanwhile, for low-mass discs with negligible accretion on to the tertiary, Martin et al. (2016) demonstrated that the tertiary can remain at large mutual inclinations or even be pumped to large inclinations via secular oscillations.

The combination of the tertiary accreting most of the mass and angular momentum from the surrounding disc explains the observed

[13]Note, however, that the Borkovits et al. (2016) ETV solution for KIC 4055092 should be considered only with considerable caution, as it gives an outer period of $P_{\rm out} \approx 31.6$ yr, which is ~8 times longer than the duration of the analysed *Kepler* data set.

anticorrelation between $q_{\rm out}$ and $i_{\rm mut}$. Accretion from a massive disc will substantially increase $q_{\rm out}$ while dissipating the triple towards coplanarity. Moreover, compact triples that formed via two episodes of disc fragmentation should be especially coplanar, perhaps explaining the excess of triply eclipsing systems with $i_{\rm mut} < 4^\circ$ relative to moderately misaligned triples, albeit an observational selection bias could also play a role. Meanwhile, a tertiary that is captured by a low-mass disc late in the formation of the system will accrete only marginal additional mass and its inclination with respect to the inner binary will change only slightly. Hence the observed population of low-mass tertiaries tend to have large mutual inclinations.

## 6 CONCLUSIONS

In this paper, we have carried out complex photodynamical analyses of four compact, tight, hierarchical triple stellar systems. These systems were observed quasi-continuously with high photometric precision by the *Kepler* spacecraft during its 4-yr-long prime mission, and then were more recently revisited with the *TESS* space telescope. All four triples consist of currently eclipsing, eccentric inner binaries which, due to strong third-body interactions and the non-alignment of the inner and outer orbits, produce rapid and large amplitude eclipse timing and depth variations. These serve as ideal targets for precise, in-depth dynamical analyses. Moreover, one of the four targets, KIC 6964043, also exhibits third-body eclipses, thereby allowing further refinements of the system parameters.

On the other hand, unfortunately, due the faintness of the systems, no RV measurements are available for any of them. Thus, we used an analysis of the composite system SED in combination with astrophysical-model dependent PARSEC isochrones as proxies for the determination of the individual stellar masses and, indirectly, radii. In such a manner, we were able to obtain fundamental stellar parameters with accuracies of about $2-8$ per cent. This relatively lower accuracy in these physical stellar parameters, however, does not affect our main purpose of mapping the full 3D configurations of the triples and their dynamics with unprecedentedly high precision. This results from the fact that the geometry and dynamics of the systems are mainly determined by such relative dimensionless quantities as the mass ratios and the orbital positions of the bodies relative to each other. Thus, we were able to determine the orbital elements, both in the observational and the dynamical frames of references, for all systems and subsystems with precisions of better than 1 per cent. Here, we mainly highlight the precise determinations not only of the mutual inclination angles, but also of the current positions of the dynamical lines of apsides, and dynamical nodes. These are direct important key parameters in the equations of secular perturbation theory and, hence, in addition to the mutual inclination of the orbits and the ratios of the masses and separations (periods), they substantially influence the future dynamical evolution of the systems. Thus, knowing these parameters, we were able to model realistically the future dynamical, and corresponding astrophysical, evolution of the four triple systems.

Two of the four triples, KICs 6964043 and 5653126, were found to be practically flat. In these systems, our short-term numerical integrations have shown only minor orbital variations in the forthcoming 1 million yr, despite the fact that KIC 6964043 is an extremely tight triple system. On the other hand, integrating the secular dynamical evolution of these systems over longer time-scales, we find that KIC 6964043 is expected to become dynamically unstable and most likely dissolve within the next 1 Gyr. In contrast to this scenario, KIC 5653126 will pass through two common envelope phases and also stellar merger(s) before it will end its life most likely as a single white dwarf.

The other two systems, KICs 5731312 and 8023317, were demonstrated to belong to the high mutual inclination regime, at least in the sense of the original ZKL theory. To the best of our knowledge, KIC 8023317 has the second highest accurately known mutual inclination angle among the known hierarchical triple stellar systems. (The highest mutual inclination system is Algol, where the outer orbit is nearly perpendicular to the inner one; Lestrade et al. 1993; Csizmadia et al. 2009; Zavala et al. 2010.) According to our short-term numerical integrations, both inclined KIC triple systems exhibit characteristic, quasi-sinusoidal variations in their inner eccentricities and mutual inclinations (*e*-cycles of the ZKL-theorem) on some hundred-year-long time-scales, with amplitudes of 10–30 per cent of the entire physically meaningful range of these parameters. Moreover, while the dynamical lines of apsides of the inner pair in KIC 5731312 circulates (though this circulation has superposed on it some librations), KIC 8023317 exhibits clear libration, at least during the forthcoming 1 million yr. On the other hand, the observable apsidal motion in both of these highly mutually inclined systems is retrograde, which make these EBs more exotic. Similar to the previous, almost flat systems, the final fates of these triples are driven again by the masses of their components. Our secular dynamical evolution studies predict that the low-mass triple KIC 5731312 will also become unstable on a Gyr time-scale, and most probably, the less-massive tertiary will be ejected from the system. Finally, the evolution of the more massive triple KIC 8023317 is expected to resemble that of KIC 5653126 with the difference in this case being that the most probable final remnant may be a cataclysimic variable instead of a single white dwarf.

Due to the non-alignment of the inner and outer orbits, all four targets exhibit rapid orbital precession and hence, EDVs. As a consequence, none of the four inner binaries remain eclipsing during their complete precession cycle. In this regard, the nearly flat system, KIC 6964043, is the least affected, as its inner pair will display eclipses over the vast majority of its precession cycle. In the case of the other three systems, they will exhibit regular, inner eclipses only during short portions of their $\sim$200–1400 yr-long precession cycles. Naturally, this implies that there may be numerous similar tight compact systems that are currently in non-eclipsing phases, but which can be discovered as EBs in the near or far future.

What is more interesting is that our photodynamical results predict that all four systems may well exhibit third-body eclipses during some shorter or longer phases of their complete precession cycles. In this regard, KIC 6964043 is exceptional in the sense that it continuously displays third-body eclipses. We further note that this system is similar to the vast majority of the presently known triply eclipsing triple systems, which were found to be practically flat and, hence, they continuously exhibit regular inner as well as third-body eclipses. One might therefore think that finding third-body eclipses in EBs is just an observational selection effect, since EBs are naturally more intensively observed and followed than non-eclipsing stars. By this reasoning, there would be a much smaller chance to discover serendipitously third-body eclipses in the case of a target that exhibits neither regular eclipses nor some other kind of characteristic light variations which would make it worthy of frequent observations. It turns out that finding third-body eclipses in EBs is indeed a selection effect, but not simply because EBs tend to be better studied. In Rappaport et al. (2022), we discussed the fact that substantially more triply eclipsing triples were found in a visual survey of $\sim 10^6$ preselected EBs than in $\sim 10^7$ random stars, all taken from the *TESS* full frame images. The selection effects involved

include the facts that: (i) the more compact triple systems that we are studying (i.e. with $P_{\rm out} \lesssim 1000$ d) are expected to be nearly flat (see Section 5.5); (ii) the shorter the outer period in a triple system (i.e. the more compact), the wider the outer inclination domain where third-body eclipses may occur; and (iii) once an EB has been found, it is already somewhat preferentially aligned so as to increase the eclipse pobability of an outer triple star. Therefore, in such a manner, the enhancement of the third-body eclipsers amongst the EBs (forming *triply* eclipsing triples) may be an indirect consequence of the formation mechanism(s) of most compact triples, i.e. one that produces practically flat systems.

Our results show that there might be a fair number of episodically appearing third-body eclipser systems amongst inclined compact triple systems.[14] The cases of KIC 2835289 and TIC 167692429 were already mentioned above (Section 5.2). We note, furthermore, that we have also found a few more solo third-body eclipse-like events in the *TESS* observations of other currently non-eclipsing targets, and one such event was especially noteworthy for being detected in the light curve of a former EB, V699 Cygni.[15] Further investigations of these events are in progress.

Finally we discuss briefly the possible connection of our findings with the different formation scenarios of multiple systems. What is quite evident at first sight is that the mass ratios are markedly different for the flat and the inclined systems, which may imply different formation scenarios.

## ACKNOWLEDGEMENTS

TB acknowledges the support of the PRODEX Experiment Agreement No. 4000137122 between the ELTE Eötvös Loránd University and the European Space Agency (ESA-D/SCI-LE-2021-0025), and the support of the city of Szombathely.

ST acknowledges support from the Netherlands Research Council NWO (VENI 639.041.645 and VIDI 203.061 grants).

The operation of the BRC80 robotic telescope of Baja Astronomical Observatory has been supported by the project 'Transient Astrophysical Objects' GINOP 2.3.2-15-2016-00033 of the National Research, Development, and Innovation Office (NKFIH), Hungary, funded by the European Union.

This paper includes data collected by the *TESS* mission. Funding for the *TESS* mission is provided by the NASA Science Mission directorate. Some of the data presented in this paper were obtained from the Mikulski Archive for Space Telescopes (MAST). STScI is operated by the Association of Universities for Research in Astronomy, Inc., under NASA contract NAS5-26555. Support for MAST for non-*HST* data is provided by the NASA Office of Space Science via grant NNX09AF08G and by other grants and contracts.

This work has made use of data from the European Space Agency (ESA) mission *Gaia*,[16] processed by the *Gaia* Data Processing and Analysis Consortium (DPAC).[17] Funding for the DPAC has been provided by national institutions, in particular the institutions participating in the *Gaia* Multilateral Agreement.

This publication makes use of data products from the Wide-field Infrared Survey Explorer, which is a joint project of the University of California, Los Angeles, and the Jet Propulsion Laboratory/California Institute of Technology, funded by the National Aeronautics and Space Administration.

This publication makes use of data products from the Two Micron All Sky Survey, which is a joint project of the University of Massachusetts and the Infrared Processing and Analysis Center/California Institute of Technology, funded by the National Aeronautics and Space Administration and the National Science Foundation.

We used the Simbad service operated by the Centre des Données Stellaires (Strasbourg, France) and the ESO Science Archive Facility services (data obtained under request number 396301).

This research made use of LIGHTKURVE, a PYTHON package for *Kepler* and *TESS* data analysis (Lightkurve Collaboration 2018).

This research made use of ASTROPY,[18] a community-developed core PYTHON package for Astronomy (Astropy Collaboration 2013, 2018).

This research made use of ASTROQUERY: an Astronomical Web-Querying Package in PYTHON (Ginsburg et al. 2018).

## DATA AVAILABILITY

The *TESS* data underlying this article were accessed from MAST (Barbara A. Mikulski Archive for Space Telescopes) Portal (https://mast.stsci.edu/portal/Mashup/Clients/Mast/Portal.html). The ASAS-SN archival photometric data were accessed from https://asas-sn.osu.edu/. The ATLAS archival photometric data were accessed from https://fallingstar-data.com/forcedphot/queue/. A part of the data were derived from sources in public domain as given in the respective footnotes. The derived data generated in this research and the code used for the photodynamical analysis will be shared on reasonable request to the corresponding author.

## REFERENCES

Abdul-Masih M. et al., 2016, AJ, 151, 101
Astropy Collaboration, 2013, A&A, 558, A33
Astropy Collaboration, 2018, AJ, 156, 123
Auvergne M. et al., 2009, A&A, 506, 411
Bailer-Jones C. A. L., Rybizki J., Fouesneau M., Demleitner M., Andrae R., 2021, AJ, 161, 147
Bate M. R., 2018, MNRAS, 475, 5618
Bate M. R., Bonnell I. A., 1997, MNRAS, 285, 33
Borkovits T., 2022, Galaxies, 10, 9
Borkovits T., Forgács-Dajka E., Regály Z., 2007, A&A, 473, 191
Borkovits T. et al., 2013, MNRAS, 428, 1656
Borkovits T., Rappaport S., Hajdu T., Sztakovics J., 2015, MNRAS, 448, 946
Borkovits T., Hajdu T., Sztakovics J., Rappaport S., Levine A., Bíró I. B., Klagyivik P., 2016, MNRAS, 455, 413
Borkovits T. et al., 2018, MNRAS, 478, 513
Borkovits T. et al., 2019a, MNRAS, 483, 1934
Borkovits T., Sperauskas J., Tokovinin A., Latham D. W., Csányi I., Hajdu T., Molnár L., 2019b, MNRAS, 487, 4631
Borkovits T., Rappaport S., Hajdu T., Maxted P. F. L., Pál A., Forgács-Dajka E., Klagyivik P., Mitnyan T., 2020a, MNRAS, 493, 5005
Borkovits T. et al., 2020b, MNRAS, 496, 4624
Borkovits T. et al., 2021, MNRAS, 503, 3759
Borkovits T. et al., 2022, MNRAS, 510, 1352
Borucki W. J. et al., 2010, Science, 327, 977

[14] This situation partially resembles the findings of Martin & Triaud (2015) who claimed that most of the inclined circumbinary planets orbiting EBs should produce transits for shorter or longer times during their orbital precession cycles.

[15] Shortly before the submission of this manuscript, the discovery of a likely third-body eclipse in the former, but no-longer EB V699 Cygni, was also reported independently by Zasche, Henzl & Masek (2022)

[16] https://www.cosmos.esa.int/gaia

[17] https://www.cosmos.esa.int/web/gaia/dpac/consortium

[18] http://www.astropy.org

Bressan A., Marigo P., Girardi L., Salasnich B., Dal Cero C., Rubele S., Nanni A., 2012, MNRAS, 427, 127
Camacho J., Torres S., García-Berro E., Zorotovic M., Schreiber M. R., Rebassa-Mansergas A., Nebot Gómez-Morán A., Gänsicke B.T, 2014, A&A, 566, A86
Carter J. A. et al., 2011, Science, 331, 562
Conroy K. E., Prša A., Stassun K. G., Orosz J. A., Fabrycky D. C., Welsh W. F., 2014, AJ, 147, 45
Conroy K. E., Prša A., Stassun K. G., 2015, in Rucinski S. M., Torres G., Zejda M., eds, ASP Conf. Ser. Vol. 496, Living Together: Planets, Host Stars and Binaries, Astron. Soc. Pac., San Francisco, p. 99
Csizmadia Sz. et al., 2009, ApJ, 705, 436
Csizmadia Sz., Smith A. M. S., Cabrera J., Klagyivik P., Chaushev A., Lam K. W. F., 2021, A&A, preprint (arXiv:2108.11822)
Cutri R.M. et al., 2013, wise.rept, 1C
Czekala I., Chiang E., Andrews S. M., Jensen E. L. N., Torres G., Wilner D. J., Stassun K. G., Macintosh B., 2019, ApJ, 883, 22
de Kool M., 1990, ApJ, 358, 189
El-Badry K., Rix H.-W., Tian H., Duchêne G., Moe M., 2019, MNRAS, 489, 5822
Fabrycky D., Tremaine S., 2007, ApJ, 669, 1298
Farris B. D., Duffell P., MacFadyen A. I., Haiman Z., 2014, ApJ, 783, 134
Ford E. B., 2005, AJ, 129, 1706
Ford E. B., Kozinsky B., Rasio F. A., 2000, ApJ, 535, 385
Foucart F., Lai D., 2014, MNRAS, 445, 1731
Gaia Collaboration, 2021, A&A, 649, A1
Gimenez A., Garcia-Pelayo J. M., 1983, Ap&SS, 92, 203
Ginsburg A. et al., 2019, AJ, 157, 98
Greiss S. et al., 2012, AJ, 144, 24
Harrington R. S., 1968, AJ, 73, 190
Henden A. A., 2019, J. Am. Assoc. Var. Star Obs., 47, 130
Henden A. A., Levine S., Terrell D., Welch D., 2015, American Astronomical Society, AAS Meeting #225. id.336.16
Ito T., Ohtsuka K., 2019, Monogr. Environ. Earth Planets, 7, 1
Ivanova N., et al., 2013, A&AR, 21, 59
Jordi C. et al., 2010, A&A, 523, A48
Kirk B. et al., 2016, AJ, 151, 68
Kiseleva L. G., Eggleton P. P., Mikkola S., 1998, MNRAS, 300, 292
Klinglesmith D. A., Sobieski S., 1970, AJ, 75, 175
Kozai Y., 1962, AJ, 67, 591
Lestrade J.-F., Phillips R. B., Hodges M. W., Preston R. A., 1993, ApJ, 410, 808
Lidov M. L., 1962, Planet. Space Sci., 9, 719
Lightkurve Collaboration, 2018, Astrophysics Source Code Library. record ascl:1812.013
Livio M., Soker N., 1988, ApJ, 329, 764
Lodato G., Facchini S., 2013, MNRAS, 433, 2157
Lubow S. H., Ogilvie G. I., 2000, ApJ, 538, 326
Lucy L. B., 1967, Z. Astrophys., 65, 89
Mardling R. A., Aarseth S. J., 2001, MNRAS, 321, 398
Martin D. V., Triaud A. H. M. J., 2015, MNRAS, 449, 781
Martin R. G., Lubow S. H., Nixon C., Armitage P. J., 2016, MNRAS, 458, 4345
Martin R. G., Zhu Z., Armitage P. J., 2020, ApJ, 898, L26
Mazeh T., Shaham J., 1979, A&A, 77, 145
Meibom S., Mathieu R. D., 2005, ApJ, 620, 970
Mitnyan T., Borkovits T., Rappaport S., Pál A., Maxted P. F. L., 2020, MNRAS, 498, 6034
Moe M., Di Stefano R., 2017, ApJS, 230, 15
Moe M., Kratter K. M., 2018, ApJ, 854, 44
Naoz S., 2016, ARA&A, 54, 441
Naoz S., Fabrycky D. C., 2014, ApJ, 793, 137
Naoz S., Farr W. M., Lithwick Y., Rasio F. A., Teyssandier J., 2013, MNRAS, 431, 2155
Offner S. S. R., Moe M., Kratter K. M., Sadavoy S. I., Jensen E. L. N., Tobin J. J., 2022, preprint (arXiv:2203.10066)
Paczynski B., 1976, in Eggleton P., Mitton S., Whelan J., eds, Structure and Evolution of Close Binary Systems. Reidel, Dordrecht
Paegert M., et al., 2021, preprint (arXiv:2108.04778)
Pál A., 2012, MNRAS, 421, 1825
Papaloizou J. C. B., Terquem C., 1995, MNRAS, 274, 987
Prša A., Zwitter T., 2005, ApJ, 628, 426
Rappaport S., Deck K., Levine A., Borkovits T., Carter J., El Mellah I., Sanchis-Ojeda R., Kalomeni B., 2013, ApJ, 768, 33
Rappaport S. et al., 2022, MNRAS, 513, 4341
Ricker G.R. et al., 2015, J. Astron. Telesc. Intrum. Syst., 1, 014003
Skrutskie M. F. et al., 2006, AJ, 131, 1163
Söderhjelm S., 1975, A&A, 42, 229
Söderhjelm S., 1982, A&A, 107, 54
Tobin J. J. et al., 2016, Nature, 538, 483
Tokovinin A. A., 2000, A&A, 360, 997
Tokovinin A., 2014, AJ, 147, 87
Tokovinin A., 2018, AJ, 155, 160
Tokovinin A., 2021, Universe, 7, 352
Tokovinin A., Moe M., 2020, MNRAS, 491, 5158
Toonen S., Nelemans G., 2013, A&A, 557, A87
Toonen S., Hamers A., Portegies Zwart S., 2016, Comput. Astrophys., 3, 6
Toonen S., Portegies Zwart S., Hamers A. S., Bandopadhyay D., 2020, A&A, 640, A16
Toonen S., Boekholt T. C. N., Portegies Zwart S., 2022, A&A, 661, A61
von Zeipel H., 1910, Astron. Nachr., 183, 345
Webbink R., 1984, ApJ, 277, 355
Young M. D., Clarke C. J., 2015, MNRAS, 452, 3085
Zanazzi J. J., Wu Y., 2021, AJ, 161, 263
Zasche P., Henzl Z., Masek M., 2022, A&A, preprint (arXiv:2205.03934)
Zavala R. T., Hummel C. A., Boboltz D. A., Ojha R., Shaffer D. B., Tycner C., Richards M. T., Hutter D. J., 2010, ApJ, 715, L44
Zorotovic M., Schreiber M. R., 2022, MNRAS, 513, 3587
Zorotovic M., Schreiber M. R., Gänsicke B. T., Nebot Gómez-Morán A., 2010, A&A, 520, A86

## SUPPORTING INFORMATION

Supplementary data are available at *MNRAS* online.

**Table B1.** Binary Mid Eclipse Times for KIC 6964043.
**Table B2.** Binary Mid Eclipse Times for KIC 5653126.
**Table B3.** Binary Mid Eclipse Times for KIC 5731312.
**Table B4.** Binary Mid Eclipse Times for KIC 8023317.

Please note: Oxford University Press is not responsible for the content or functionality of any supporting materials supplied by the authors. Any queries (other than missing material) should be directed to the corresponding author for the article.

## APPENDIX A: DETERMINATION OF THE LIMITS OF THE INCLINATION DOMAIN WHERE THIRD-BODY ECLIPSES MIGHT OCCUR

In order to find reasonable estimations for the inclination limits of the occurrence of third-body eclipses, we follow the same formalism as was used formerly in appendix A of Borkovits et al. (2013). There, we have shown that using the formalism of Jacobian position vectors, the spatial distances of the centres of the three stars can be calculated as

$$\vec{d}_{\rm AaAb} = \vec{\rho}_1 \tag{A1}$$

$$\vec{d}_{\rm AaB} = \vec{\rho}_2 + \frac{q_1}{1+q_1}\vec{\rho}_1 \tag{A2}$$

$$\vec{d}_{\rm AbB} = \vec{\rho}_2 - \frac{1}{1+q_1}\vec{\rho}_1, \tag{A3}$$

respectively.[19] Let's use an observational frame of reference in which the origin is the centre of mass of the inner binary, 'X-Y' is the tangential plane of the sky, and 'Z' axis is directed away from the observer. Then the Cartesian coordinates of the first two Jacobians can be written as

$$x = \rho[\cos u \cos\Omega - \sin u \sin\Omega \cos i], \tag{A4}$$

$$y = \rho[\cos u \sin\Omega + \sin u \cos\Omega \cos i], \tag{A5}$$

$$z = \rho \sin u \sin i, \tag{A6}$$

where $u$ denotes the longitude of second/third body (to which the first/second Jacobian points) along the given orbit, measured from the ascending node. (In the eccentric case $u = v + \omega$, where $v$ stands for the true anomaly.) Then, the sky-projected distances can readily be obtained as

$$d^{xy}_{\rm AaAb} = \rho_1 \sqrt{1 - \sin^2 i_1 \sin^2 u_1}, \tag{A7}$$

$$\begin{aligned} d^{xy}_{\rm AbB} = \rho_2 \Bigg[ & 1 - \sin^2 i_2 \sin^2 u_2 \\ & - 2\frac{1}{1-q_1}\left(\lambda - \sin i_1 \sin u_1 \sin i_2 \sin u_2\right) \\ & + \left(\frac{1}{1+q_1}\frac{\rho_2}{\rho_1}\right)^2 \left(1 - \sin^2 i_1 \sin^2 u_1\right) \Bigg]^{1/2}, \end{aligned} \tag{A8}$$

where $\lambda$ denotes the direction cosine between the two Jacobian vectors. Note, the expression referring to distance $d^{xy}_{\rm AaB}$ is not shown, however, one can obtain it very easily by replacing $-1/(1+q_1)$ with $q_1/(1+q_1)$.) It is clear that eclipses may occur when the sky-projected distances of any of the two bodies become less than the sum of their radii. For regular two-body eclipses, equation (A7) leads readily to the usual condition of $R_1 + R_2 \geq a|\cos i|$, which is, however, strictly valid only for circular orbits. It also directly follows that at times of mid-eclipse, $u_1 = \pm\pi/2$. In eccentric, not exactly edge-on cases, however, the smallest distance may occur somewhat earlier or later than the conjunction occurs. The departure is, however, in almost all cases, small, and therefore, negligible (Gimenez & Garcia-Pelayo 1983). Thus, when we calculated and utilized the condition given by equation (2) for the inner eclipses, we were working with the conjunction points (i.e. $u_1 = \pm\pi/2$).

The case of third-body eclipses is much more complex, and no robust, exact condition(s) can be given. Thus, we adopted the following assumptions. Again, one can expect third-body eclipses around the conjunctions of the outer orbit. Hence, we arbitrarily set $u_2 = \pm\pi/2$. At these times, the projection of the second Jacobian vector on to the plane of the sky becomes

$$\vec{\rho}_2^{\,xy} = \rho_2 \cos i_2 (\mp \sin\Omega_2; \pm \cos\Omega_2; 0). \tag{A9}$$

Then, we look for that value of $u_1$, at which the sky-projected vector of the first Jacobian ($\vec{\rho}_1^{\,xy}$) is parallel to the former $\vec{\rho}_2^{\,xy}$, which may allow us to find the minimum sky-projected distance between the two bodies. The two vectors become parallel when their cross-product yields zero. From this condition, and assuming that $\cos i_2 \neq 0$, one can easily calculate that

$$\sin^2 u_1 = \frac{\cos^2 \Delta\Omega}{1 - \sin^2 i_1 \sin^2 \Delta\Omega}. \tag{A10}$$

Thus, one can readily find that the length of the sky-projected vector $\vec{\rho}_1^{\,xy}$ becomes

$$\rho_1^{xy} = \rho_1 \sqrt{1 - \sin^2 i_1 \sin^2 u_1} = \rho_1 \sqrt{\frac{\cos^2 i_1}{1 - \sin^2 i_1 \sin^2 \Delta\Omega}}. \tag{A11}$$

Then, as this vector is parallel to the sky-projected vector of the second Jacobian, one can write directly that

$$\begin{aligned} d^{xy}_{\rm AbB} &= \rho_2 |\cos i_2| \pm \frac{1}{1+q_1}\rho_1 |\cos i_1| \sqrt{\frac{1}{1 - \sin^2 i_1 \sin^2 \Delta\Omega}} \\ &= \rho_2 |\cos i_2| \pm \frac{1}{1+q_1}\rho_1 \sqrt{\frac{\cos^2 i_1}{\cos^2 i_1 + \sin^2 i_1 \cos^2 \Delta\Omega}} \\ &= \rho_2 |\cos i_2| \pm \frac{1}{1+q_1}\rho_1 \sqrt{\frac{1}{1 + \tan^2 i_1 \cos^2 \Delta\Omega}}. \end{aligned} \tag{A12}$$

From this last form of the expression, one can easily obtain equation (3), where we also made a further simplification, replacing $\rho_1$ with $a_1$ on the right-hand side of the equation.

## APPENDIX B: TABLES OF DETERMINED TIMES OF MINIMA FOR ALL THE FOUR SYSTEMS

In this appendix, we tabulate the individual mid-minima times of the primary and secondary eclipses, including *Kepler*, *TESS*, and ground-based observed ones, for the inner EBs of the four triples considered in this study (Tables B1-B4).

The complete Appendix B is available as supplementary material to the journal, and also in the arXiv version; here, we display only the first few lines of Table B1.

**Table B1.** Binary Mid Eclipse Times for KIC 6964043.

| BJD −2 400 000 | Cycle no. | std. dev. (*d*) | BJD −2 400 000 | Cycle no. | std. dev. (*d*) | BJD −2 400 000 | Cycle no. | std. dev. (*d*) | BJD −2 400 000 | Cycle no. | std. dev. (*d*) |
|---|---|---|---|---|---|---|---|---|---|---|---|
| 55190.173588 | 0.0 | 0.000688 | 55495.729755 | 28.5 | 0.000505 | 55796.037501 | 56.5 | 0.000497 | 56112.482348 | 86.0 | 0.000672 |
| 55195.460530 | 0.5 | 0.000538 | 55501.102486 | 29.0 | 0.000536 | 55801.369553 | 57.0 | 0.000446 | 56117.968120 | 86.5 | 0.001017 |
| 55200.886326 | 1.0 | 0.000801 | 55506.447625 | 29.5 | 0.000968 | 55806.764662 | 57.5 | 0.000393 | 56133.913187 | 88.0 | 0.000587 |
| 55206.172452 | 1.5 | 0.000961 | 55511.820059 | 30.0 | 0.000861 | 55812.101279 | 58.0 | 0.000409 | 56139.407798 | 88.5 | 0.000847 |
| 55211.601150 | 2.0 | 0.000762 | 55517.160827 | 30.5 | 0.000711 | 55822.865967 | 59.0 | 0.001426 | 56144.627374 | 89.0 | 0.000677 |
| ... | ... | ... | ... | ... | ... | ... | ... | ... | ... | ... | ... |

Integer and half-integer cycle numbers refer to primary and secondary eclipses, respectively.

This paper has been typeset from a TEX/LATEX file prepared by the author.

[19] In order to save space in this appendix, we hereafter use indices $_{1,2}$, instead of $_{\rm in,\,out}$ to distinguish parameters referring to the inner and outer orbits, respectively.